

### Contents lists available at ScienceDirect

# Energy

journal homepage: www.elsevier.com/locate/energy





# Learning based predictive control of truck platoons with speed planning

Shuyou Yu a,b, Shaoyu Sun a, Hong Chen a,c, Yangfan Liu a, Wenbo Li a,\*, Jung-Su Kim b

- <sup>a</sup> The Department of Control Science and Engineering, Jilin University, Changchun 130025, China
- b The National Key Laboratory of Automotive Chassis Integration and Bionics, Jilin University, Changchun 130025, China
- <sup>c</sup> The College of Electronics and Information Engineering, Tongji University, Shanghai 200092, China
- d The Department of Electrical and Information Engineering, Seoul National University of Science and Technology, Seoul 139-743, South Korea

## ARTICLE INFO

Keywords:
Truck platoon
Fuel consumption
Speed planning
Reinforcement learning
Distributed model predictive control

## ABSTRACT

Connectivity and autonomy stand out as two highly promising technologies for fuel efficiency in the realm of automated transportation. This paper addresses the issue of fuel consumption in autonomous truck platoons and introduces a hierarchical framework. Within the speed planning layer, a fuel consumption model for the leading truck is formulated to compute velocity profile. Simultaneously, a distributed learning-model predictive control (DL-MPC) method is employed to ensure the cohesive movement of a truck platoon in a predefined formation. The co-simulation platform, leveraging Trucksim and Simulink, provides a comprehensive environment for assessing and validating the proposed control strategy. Comparison experiments validate the effectiveness of the proposed method. Distributed model predictive control (DMPC) and two-delay deep deterministic policy gradient (TD3) algorithms are conducted to illustrate the advantages of the controller in terms of control performance and computation time. The speed planning method outperforms constant speed, experience-based speed setting, and reinforcement learning-based speed planning in terms of fuel efficiency. Furthermore, the energy-saving effect of the proposed strategy is verified from the perspective of engine fuel characteristics. Therefore, the framework proposed in this paper ensures excellent control performance and fuel economy of truck platoon while reducing the computation time of the controller.

### 1. Introduction

As the logistics industry develops, the number of trucks is increasing, resulting in higher fossil fuel consumption and emissions [1]. Urban fine particulate concentration in China reaches 51 micrograms/ cubic meter, which is six times greater than that of the United States. and China aims to reduce CO2/GDP by 60%-65% below 2005 by 2030 adhering to The Paris Agreement. There is no doubt that lower fuel consumption leads to cost savings for truck platoons, and it also reduces emissions [2,3]. Platooning has the potential to improve road safety by significantly reducing reaction times and minimizing for the likelihood human error within the platoon, which can decrease rearend crashes [4]. Currently, the focus of research lies in minimizing energy consumption while ensuring the safety of truck platoons [5,6]. The comparison between the proposed work and existing studies are summarized in Table 1. As shown in the table, studies [3,7-11] have achieved fuel saving and longitudinal control but exhibit shortcomings in computational efficiency and lateral control. Studies [12-15] focus on both longitudinal and lateral control but do not address computational efficiency and speed planning. Meanwhile, studies [16-19] explore computational efficiency and both longitudinal and lateral

control but overlook speed planning and energy efficiency. In contrast, the proposed work in this study comprehensively addresses four key aspects – computational efficiency, fuel consumption, longitudinal control, and lateral control – effectively filling a critical gap in existing research.

## 1.1. Motivation

Although extensive research has been conducted on truck platooning control, several critical gaps remain. First, although most existing works focus primarily on longitudinal control for fuel efficiency [3,20], the coupling between longitudinal and lateral dynamics should not be neglected under real-world driving conditions. Second, distributed model predictive control (DMPC) has been widely adopted [16], yet its high computational burden poses challenges for large-scale real-time applications. Third, speed planning strategies for the leading truck often fail to account for the dynamic constraints of following trucks [21], resulting in impractical trajectories that cannot be reliably executed. These gaps highlight the necessity of developing a unified control framework that (i) explicitly accounts for coupled

E-mail address: liwb21@mails.jlu.edu.cn (W. Li).

<sup>\*</sup> Corresponding author.

**Table 1**Comparing the proposed work with previous studies.

Studies	Computational efficiency	Fuel consumption	Longitudinal control	Lateral control
[3,7–11]	×			×
[12–15]	X	×	$\checkmark$	$\checkmark$
[16-19]	$\sqrt{}$	×	V	V
Proposed work		$\checkmark$	$\sqrt{}$	

longitudinal-lateral dynamics, (ii) enhances the computational efficiency of DMPC-based methods for real-time implementation, and (iii) integrates speed planning with the physical tracking capabilities of following trucks.

Motivated by these challenges, this study addresses truck platooning control by jointly considering fuel economy, coupled longitudinal-lateral dynamics, and computational efficiency. A two-layer control framework is designed, with the upper layer focused on speed planning for the leading truck, aimed at fuel-efficient speed profiles. With the lower layer, i.e., the platoon control layer, the distributed learning-model predictive controller (DL-MPC) is designed to ensure platoon safety.

## 1.2. Contributions

This paper makes several key contributions, which are outlined as follows:

- (1) This paper proposes a speed planning strategy for the leading truck that incorporates both road information and the tracking capability of following trucks. The proposed approach explicitly integrates the dynamic response limits of following trucks into the speed planning process, thereby improving overall fuel efficiency and safety of the platoon.
- (2) This paper develops a DL-MPC framework for longitudinal and lateral control of truck platoons, which represents a novel integration of traditional control methods and artificial intelligence. The proposed framework ensures efficient, safe, and coordinated movement of truck platoons in dynamic environments. This innovative approach enhances the system's ability to respond to real-time changes in traffic and road conditions.
- (3) The proposed method retains the control performance of traditional DMPC algorithm while possessing the efficient solving performance of neural networks. Comparing with DMPC and two-delay deep deterministic policy gradient (TD3) algorithms, the proposed method can guarantee the control performance and reduce the computation time.

## 1.3. Paper organization

The paper proceeds as follows: In Section 2, the relevant works are introduced. In Section 3, the longitudinal and lateral coupling dynamics model of trucks are established, a fuel consumption model of the leading truck is established, the platoon model and the control objectives are proposed, respectively. In Section 4, speed planning program of the leading truck is designed and a DL-MPC algorithm is designed. The tracking control performance and the fuel consumption of the platoon are presented in Section 5. Section 6 concludes the paper.

## 2. Related work

The analysis of fuel consumption in truck platoons has been extensively studied and can be divided into three primary approaches: vehicle spacing, traffic oscillation and speed planning [22]. In vehicle spacing approach, the correlation between the air resistance coefficient and the distance between the trucks is presented in [23,24]. These studies indicate that the average resistance of the platoon decreases as the spacing between trucks narrows, enabling greater fuel savings

with reduced spacing [23]. In [24], the relationship between fuel consumption and vehicle gap is studied, which shows that the fuel saving rate can reach 15% when the gap is maintained at 4.7 m. The traffic oscillation method examines fuel consumption in scenarios with frequent accelerations. In [25], in order to avoid unnecessary braking and acceleration during truck traveling, the minimum acceleration of the truck from static to set speed is studied. A reinforcement learning (RL) approach to fuel consumption analysis in traffic oscillation scenarios is presented in [26].

Speed planning approaches include methodologies such as dynamic program, back-step control, model predictive control and RL. In [27], a novel development of an ecological driving system for traveling a vehicle on roads with up-down slopes is presented. In [28], a cooperative control strategy is presented that takes into account preview information, which can achieve fuel savings of up to 14% on a steep descent compared to the adaptive cruise control system. In [29], a control objective is to maximize fuel economy by controlling a safe following distance or cruising at the optimum speed under constrained driving torque conditions. In [30], dynamic programming is used to calculate the optimal fuel-efficient speed of the platoon, and a distributed model predictive control framework is developed to control the trucks in real time. The results show that the fuel consumption of the following trucks can be reduced by 12%. A two-level hierarchical framework for a truck platoon coordination has been presented in [31], which designs a discrete-time back-step control law based on a nonlinear vehicle model that considers road gradient and vehicle heterogeneity, and strengthens the control law with a novel string stability criterion. In [32], a distributed model predictive control method is designed for the fuel-efficiency of heavy-duty trucks, and the fuel saving of the proposed control strategy is studied by simulation. In [33], a low-cost predictive cruise control method is presented. The method achieves energy savings of 8% to 10% compared to conventional adaptive cruise control when testing on a real truck test platform. In [34], a RL approach is used to train vehicles to keep safe spacing and reduce fuel consumption by setting the reward function.

Most of the previous studies have focused on speed planning and energy-saving control for the longitudinal dynamics of the platoons [35]. However, in practical applications, lateral dynamics should also be considered in addition to longitudinal dynamics. A multi-objective integrated control structure is designed to coordinate lateral and longitudinal motion control in [36], encompassing a global cooperative control layer, a control allocation layer, and an action execution layer. The dynamics model of the vehicle's longitudinal and lateral coupling characteristics is established, and the nonlinear controllers for longitudinal and automatic steering based on nonlinear model predictive control are designed, respectively [37]. Based on the six-degree-offreedom vehicle dynamics model, a new integrated control system for longitudinal, lateral and vertical is proposed in [38]. The system is based on model predictive control and can also consider operability.

Truck platoons usually operate in complex traffic environments rather than isolated highways. Platoon control must handle additional challenges, including mixed traffic with human-driven vehicles, uncertain driver behaviors, traffic signals, and disturbances from communication. Some studies have addressed some of these issues, such as merge-diverge coordination [39–41], multi-platoon cooperation [42, 43], and the influence of road surface [44,45].

In addition, communication is an another critical factor. Communication delays have been extensively studied [46,47]. More challenging

communication scenarios, such as packet loss, topology switching, and denial-of-service (DoS) attacks, have also been investigated, where adaptive and switching-based control laws were designed to maintain tracking performance and safety [48–50]. Some works propose distributed detection and recovery mechanisms, as well as security-aware topology reconfiguration strategies, to enhance resilience against disturbances [51,52]. These studies suggest that extending platoon control strategies to account for complex traffic interactions, communication uncertainties, and security threats is essential for practical deployment.

Due to the strong nonlinearity of the longitudinal and lateral dynamics coupling model, the model predictive control has a huge computational burden when solving the optimization problems, and the real-time performance of the platoon control cannot be guaranteed. In [53], a simplified dynamic model is obtained by ignoring the coupling component of the longitudinal driving force in the lateral dynamics, resulting in a 9.6% reduction in time. Moreover, a dual-mode DMPC strategy is proposed in [54], which can not only significantly reduce the computation time and save communication resources, but also ensure the iterative feasibility and stability of the proposed algorithm.

## 3. Problem setup

In this section, firstly, the longitudinal and lateral coupling dynamics model of the truck is established. Secondly, the fuel consumption model of the leading truck is established. Then, the longitudinal speed of the leading truck is taken as the expected speed of the platoon. Finally, the control objectives are proposed. Considering a truck platoon consists of N trucks travels on a road, where the leading truck is numbered as 0, and the following trucks are sequentially numbered from  $1 \cdots N-1$ . It is assumed that the communication network is completely reliable, i.e., there is no channel fading, packet dropout, or delay.

The hierarchical control scheme is shown in Fig. 1. The intelligent connected vehicles (ICV) achieve dual objectives of fuel efficiency optimization and safety control through the collaboration between the leading truck and the following trucks. The leading truck utilizes vehicle to infrastructure (V2I) technology to obtain road information and combines a powertrain model to compute an energy-efficient reference speed. Meanwhile, the following trucks leverage vehicle to vehicle (V2V) communication to share real-time state data and employ distributed controllers to adjust their speed and spacing, ensuring both longitudinal and lateral safety. By integrating information exchange with coordinated control algorithm, the system enables the platoon to operate with enhanced energy efficiency and safe driving performance.

## 3.1. Truck dynamics

A classical three-degree-of-freedom model [55] is adopted, in which the motion of the truck in the longitudinal, lateral and yaw directions are considered. The first-principle model of the *i*th truck is as follows:

$$\begin{cases} m_i \dot{v}_i^x - m_i v_i^y \dot{\varphi}_i = F_i^{xf} \cos \delta_i - F_i^{yf} \sin \delta_i + F_i^{xr} - F_i^f \\ m_i \dot{v}_i^y - m_i v_i^x \dot{\varphi}_i = F_i^{xf} \sin \delta_i + F_i^{yf} \cos \delta_i + F_i^{yr} \\ I_i^z \dot{\varphi}_i = \left( F_i^{xf} \sin \delta_i + F_i^{yf} \cos \delta_i \right) a_i - F_i^{yr} b_i \end{cases}$$
(1)

where  $v_i^x$ ,  $v_i^y$  and  $\dot{\varphi}_i$  are the longitudinal velocity, lateral velocity, yaw angle rate of truck. The term of  $m_i$  is the mass of truck,  $I_i^z$  is the moment of inertia around z axis,  $a_i$  and  $b_i$  are the distances from front axle and rear axle to mass center,  $\delta_i$  is the lateral control input representing steering angle of the front wheel,  $F_i^{xf}$ ,  $F_i^{xr}$ ,  $F_i^{yf}$ ,  $F_i^{yr}$  and  $F_i^f$  are the longitudinal force of front wheel, longitudinal force of rear wheel, lateral force of rear wheel and the travel resistance of the truck, respectively.

Wheel force analysis is shown in Fig. 2 and the dynamics of the wheels are:

$$\begin{cases} \dot{\omega}_i^f = \frac{T_i^d - R_w F_i^{xf}}{J_i^f} \\ \dot{\omega}_i^r = \frac{T_i^d - R_w F_i^{xr}}{J_i^r} \end{cases}$$
(2)

where  $\omega_i^f$  and  $\omega_i^r$  are the angular velocity of front and rear wheel;  $J_i^f$  and  $J_i^r$  are the moment of inertia of front and rear wheel;  $T_i^d$  is the longitudinal control input representing the torque of rear wheel;  $R_w$  is the wheel rolling radius.

Combining (1) and (2), a five-degree-of-freedom (5-DOF) dynamic model of trucks [56] is established as follows:

finder of fracks [50] is established as follows.

$$\begin{cases}
\dot{v}_i^x = v_i^y \dot{\varphi}_i + \frac{F_i^{xf} \cos \delta_i - F_i^{yf} \sin \delta_i + F_i^{xr} - F_i^f}{m_i} \\
\dot{v}_i^y = -v_i^x \dot{\varphi}_i + \frac{F_i^{xf} \sin \delta_i + F_i^{yf} \cos \delta_i + F_i^{yr}}{m_i} \\
\dot{\varphi}_i^y = \frac{\left(F_i^{xf} \sin \delta_i + F_i^{yf} \cos \delta_i\right) a_i - F_i^{yr} b_i}{I_i^z} \\
\dot{\varphi}_i^f = \frac{T_i^d - R_w F_i^{xf}}{J_i^f} \\
\dot{\varphi}_i^f = \frac{T_i^d - R_w F_i^{xr}}{J_i^f}
\end{cases}$$
(3)

Fig. 3 shows the 5-DOF dynamics model of trucks. The Pacejka tire model [57] is applied in this paper, in which the tire force can be calculated by

$$F(\chi) = D\sin\left(C\arctan\left(B\chi - E\left(B\chi - \arctan\left(B\chi\right)\right)\right)\right) \tag{4}$$

where B, C, D and E are the parameters of the tire, the input variable  $\chi$  is the slip ratio or the slip angle, and the output variable  $F(\chi)$  is the longitudinal tire force or the lateral tire force, respectively.

Note that the planar motion of trucks is considered, and the influence of roll and pitch is neglected. The load distribution between the front and rear wheels is not taken into account, and the steering angles of the left and right wheels are assumed to be equal.

To validate the effectiveness of the 5-DOF dynamic model, a comparative analysis is conducted between the model's outputs and those generated by TruckSim under identical input conditions. The input signals include a constant driving torque of 1000 N m and a sinusoidal front wheel steering angle with an amplitude of 0.01 rad. Note that the torque value of 1000 N m is chosen because it falls within the typical range of heavy-duty truck powertrains [58]. The purpose of this setting is to provide a realistic but non-extreme driving condition for validating the proposed 5-DOF dynamic model, rather than to investigate performance limits. The simulation results are presented in Fig. 4, where Figs. 4(a)–(d) show the front wheel steering angle, the longitudinal and lateral velocity, yaw rate, respectively.

To quantitatively evaluate the model fitting, three error metrics are employed: the Mean Absolute Error (MAE), the Root Mean Square Error (RMSE), and the coefficient of determination (R<sup>2</sup>). MAE measures the average absolute deviation between the predicted and measured values, providing a direct indication of the typical error magnitude, with units identical to the original data. RMSE emphasizes larger deviations by squaring the errors before averaging and taking the square root, reflecting the model's overall accuracy in the presence of occasional large errors. The term of R<sup>2</sup> is a dimensionless indicator that represents the proportion of variance in the measured data explained by the model, where values closer to 1 indicate stronger agreement. By combining absolute error metrics (MAE, RMSE) with the relative goodness-of-fit (R<sup>2</sup>), allows for a comprehensive assessment of the model's numerical accuracy and trend consistency, a comprehensive assessment of the model's numerical accuracy and trend consistency is achieved, thereby strengthening the credibility of the validation results. The performance evaluation of model fitting is summarized in Table 2.

The results indicate that under the same input conditions, the output trends of the 5-DOF dynamic model closely match those of TruckSim, with small discrepancies. This demonstrates that the proposed model effectively captures the longitudinal and lateral motion characteristics of commercial trucks, making it suitable for the controller design.

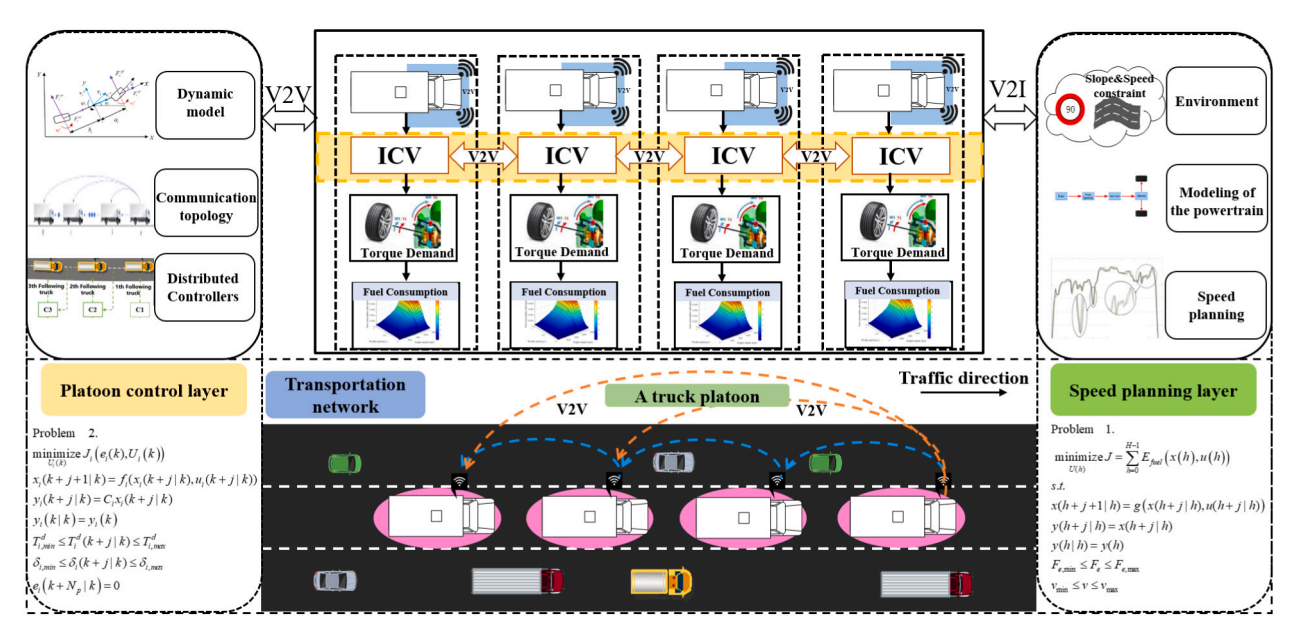


Fig. 1. The diagram for balancing fuel efficiency and safety control of the platoon.



Fig. 2. The wheel force analysis.

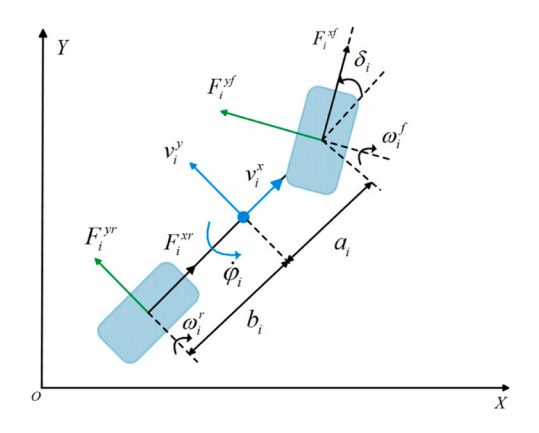


Fig. 3. The five-degree-of-freedom dynamics model of trucks.

**Table 2** Performance evaluation of model fitting.

Results	MAE	RMSE	$\mathbb{R}^2$
Front wheel steering angle	$0.31 \times 10^{-3}$ (rad)	$0.37 \times 10^{-3}$ (rad)	0.9971
Longitudinal velocity	0.025 (m/s)	0.037 (m/s)	0.9997
Lateral velocity	$6.83 \times 10^{-3} \text{ (m/s)}$	$7.83 \times 10^{-3} \text{ (m/s)}$	0.9798
Yaw rate	$2.23 \times 10^{-3} \text{ (rad/s)}$	$2.48 \times 10^{-3} \text{ (rad/s)}$	0.9731

### 3.2. Fuel consumption model of the leading truck

The fuel consumption of the truck on the slope is mainly related to the mass and the longitudinal speed. Planning the speed of the leading truck not only reduces its own fuel consumption but also enables the following trucks to track its speed, thus achieve the fuel-saving objective of the platoon. Fig. 5 shows the longitudinal dynamics of the leading truck on a slope.

Assume that any momentary variations in the performance of the engine and mechanical power can be disregarded [34]. Then, the dynamics model of the leading truck on the slope can be expressed as follows:

$$\begin{cases} \frac{ds_0}{dt} = v_0 \\ m_0 \frac{dv_0}{dt} = F_{e,0} - F_0^f \end{cases}$$
 (5)

where  $s_0$  and  $v_0$  are the position and speed of the leading truck. Note that  $F_{e,0}$  is the force provided by the engine,  $F_0^f = F_{tf,0} + F_{aero,0} + F_{gra,0}$ , in which  $F_{tf,0}$ ,  $F_{aero,0}$  and  $F_{gra,0}$  are rolling resistance, air resistance and slope resistance, and note that  $F_{tf,0} = C_{tf,0} m_0 g \cos \theta$ ,  $F_{aero,0} = \frac{1}{2} \rho C_{aero,0} A v_0^2$ ,  $F_{gra,0} = m_0 g \sin \theta$ . The term of  $C_{tf,0}$  is the rolling resistance coefficient of the leading truck,  $C_{aero,0}$ ,  $m_0$ , and A are the air resistance coefficient, the mass, and the windward aero of the leading truck, respectively. The term of  $\rho$  is the air density, g and  $\theta$  are gravity acceleration and slope angle.

The mechanical power of trucks needs to overcome the effect of gravity, and the fuel consumption of trucks is closely related to the mechanical powertrain [59]. The mechanical powertrain of the leading truck can be expressed as follows:

$$P = (F_{aero,0} + F_{gra,0} + F_{tf,0} + F_{e,0}) v_0$$
 (6)

The fuel consumption of the truck can be described as:

$$E_{fuel} = \frac{\alpha}{\gamma \cdot \beta} \left( \sigma \cdot \varepsilon \cdot \tau + P/\eta \right) \tag{7}$$

where  $E_{fuel}$  and P are the fuel consumption rate and mechanical power of the truck,  $\alpha$  is the mass ratio of fuel to air,  $\gamma$  is the calorific value of typical diesel,  $\beta$ ,  $\sigma$ ,  $\varepsilon$  and  $\tau$  are the friction coefficient, engine speed, exhaust volume and conversion factor of the engine. The term of  $\eta$  is the efficiency parameter, and  $\eta = \eta_f \cdot \eta_c$ , in which  $\eta_f$  and  $\eta_c$  are the efficiency parameters of the engine and the transmission system, respectively.

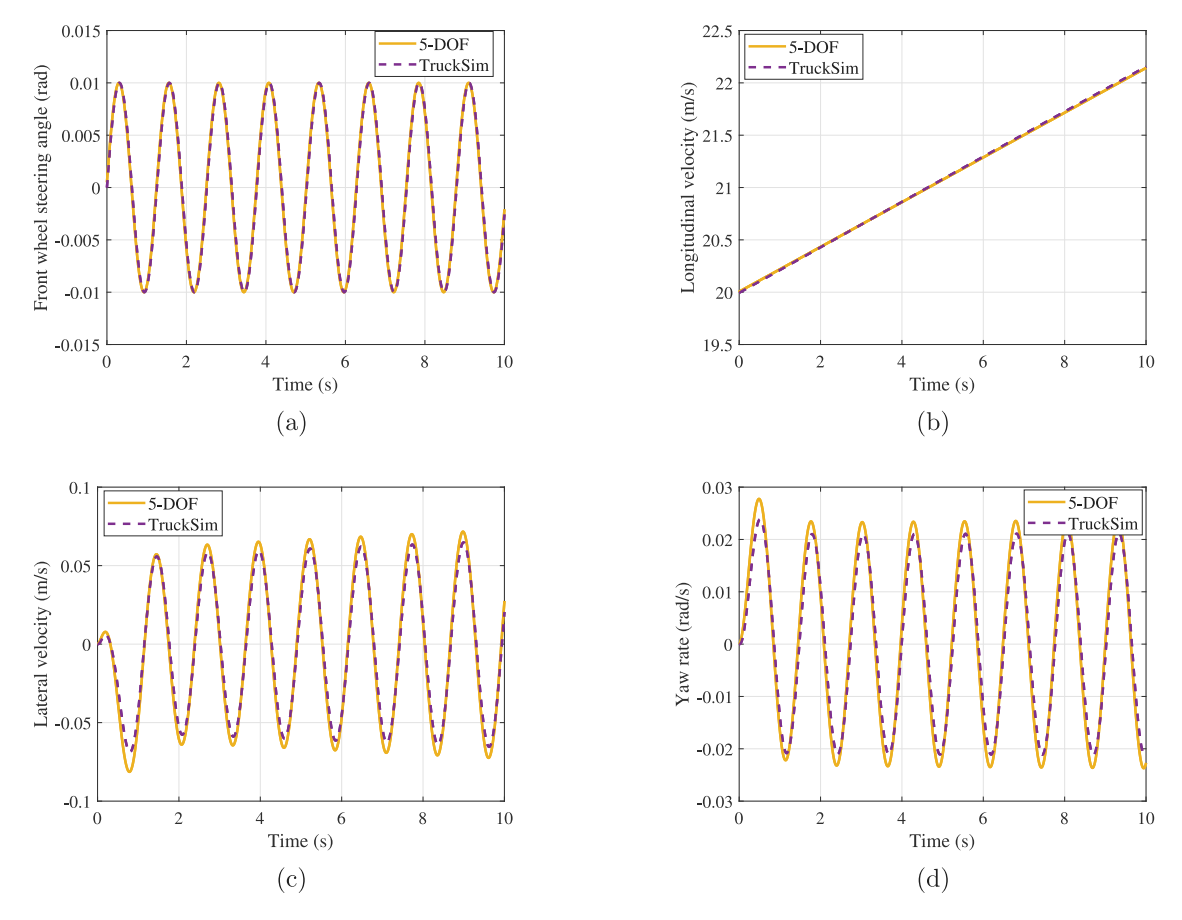


Fig. 4. Model validation experiment: (a) front wheel steering angle, (b) longitudinal velocity, (c) lateral velocity, (d) yaw rate.

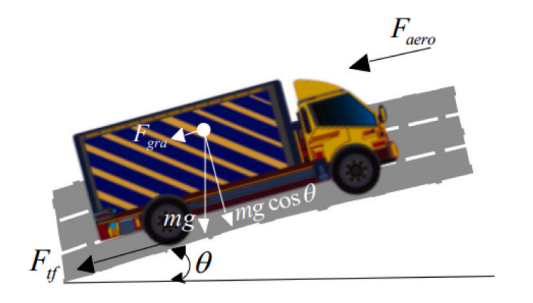


Fig. 5. The longitudinal dynamics model of the leading truck on a slope.

**Remark 1.** The actual fuel consumption of trucks is influenced by numerous external factors such as the tread and pressure of tire, weather conditions, density and humidity of air, fuel is also consumed by diesel engines when idling [27], which is almost negligible. For the sake of simplicity, in this paper, a relatively straightforward fuel consumption model is adopted that does not account for idling fuel consumption.

## 3.3. Platoon model

In order to accurately follow the required reference path, onboard sensors are essential for providing relative positional information between trucks, as well as between the truck and reference path.

To showcase varied platoon performances, truck platoon control has developed several spacing policies including constant spacing policy (CSP), constant time headway policy, and variable time headway policy [60]. To prevent the gap between trucks from amplifying as their speed increases, which results in greater fuel consumption, CSP

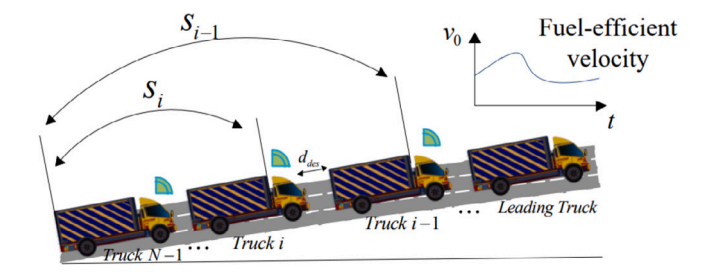


Fig. 6. The distance diagram of the truck platoon.

and predecessor-leader following information flow topology [61] are adopted in this paper.

A truck platoon is shown in Fig. 6, where  $s_i$  and  $s_{i-1}$  are the longitudinal positions of the ith following truck and the (i-1)th following truck,  $s_0$  and  $d_{des}$  are the longitudinal position of the leading truck and the desired spacing, respectively.

Fig. 7 illustrates the configuration of the lane-keeping model, where  $e_i^p$  represents the longitudinal position error, L is the preview distance,  $e_i^y$  and  $e_i^\varphi$  are the lateral position error and heading angle error, respectively, and R is the radius of the curve.

Define spacing error of the *i*th truck as:

$$e_i^p = s_i - (s_0 - id_{des}) (8)$$

Define heading error of the *i*th truck as:

$$e_i^{\varphi} = \varphi_d - \varphi_i \tag{9}$$

where  $\varphi_d$  and  $\varphi_i$  correspond to the tangential angle of lane and the actual truck heading angle.

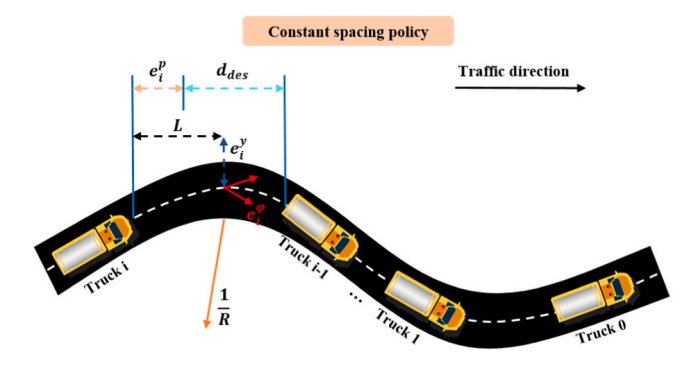


Fig. 7. The structure of the lane-keeping model.

The term of  $e_i^y$  is defined as lateral position error:

$$\dot{e}_i^y = v_i^x e_i^\varphi - v_i^y - L\dot{\varphi}_i \tag{10}$$

Combining (3), (8), (9) and (10), the integrated platoon model is as follows:

$$\begin{cases} \dot{v}_{i}^{x} = v_{i}^{y} \dot{\varphi}_{i} + \frac{F_{i}^{xf} \cos \delta_{i} - F_{i}^{yf} \sin \delta_{i} + F_{i}^{xr} - F_{i}^{f}}{m_{i}} \\ \dot{v}_{i}^{y} = -v_{i}^{x} \dot{\varphi}_{i} + \frac{F_{i}^{xf} \sin \delta_{i} + F_{i}^{yf} \cos \delta_{i} + F_{i}^{yr}}{m_{i}} \\ \ddot{\varphi}_{i} = \frac{(F_{i}^{xf} \sin \delta_{i} + F_{i}^{yf} \cos \delta_{i}) a_{i} - F_{i}^{yr} b_{i}}{I_{i}^{z}} \\ \dot{w}_{i}^{r} = \frac{T_{i}^{d} - R_{w} F_{i}^{xf}}{J_{i}^{f}} \\ \dot{w}_{i}^{r} = \frac{T_{i}^{d} - R_{w} F_{i}^{xr}}{J_{i}^{r}} \\ \dot{e}_{i}^{p} = v_{i}^{x} - v_{0}^{x} \\ \dot{e}_{i}^{y} = v_{i}^{x} e_{i}^{\varphi} - v_{i}^{y} - L\dot{\varphi}_{i} \\ \dot{e}_{i}^{\varphi} = \dot{\varphi}_{d} - \dot{\varphi}_{i} \end{cases}$$

$$(11)$$

**Remark 2.** The above problem formulation is developed under some assumptions, including homogeneous trucks, reliable communication, and known road geometry, with the application scenario restricted to highway environments. These assumptions are deliberately made to highlight the essential control objectives of platoon and to establish an optimization framework. Such a baseline setting facilitates a clear analysis of the effects of DMPC and its learning-based extension on platoon performance, and it also provides methodological insights that can be extended to more complex and uncertain traffic environments in future work.

## 3.4. Control objectives of truck platoons

This paper aims to address the problem of fuel efficiency as well as cooperative control of truck platoons using a hierarchical control structure. The objectives are as follows:

## 3.4.1. The objective of fuel saving

For the leading truck, fuel consumption is modeled by combining road information and the tracking capability of the following trucks, aiming to generate a reference speed profile for the truck platoon that minimizes fuel consumption, i.e., minimize  $E_{fuel}$ .

## 3.4.2. The objectives of platoon control

(1) The longitudinal position of the following trucks in the platoon satisfies the desired spacing policy, i.e., the longitudinal spacing error is minimized:

minimize 
$$\left\| s_i - \left( s_0 - i \cdot d_{des} \right) \right\|_2^2$$
 (12)

(2) The velocity of the *i*th following truck tracks the velocity of the leading truck, and the longitudinal velocity error between the following trucks and the leading truck is minimized:

$$\text{minimize } \left\| v_i^x - v_0^x \right\|_2^2 \tag{13}$$

where  $v_0^x$  and  $v_i^x$  are the longitudinal velocities of the leading truck and the *i*th following truck, respectively.

(3) The expected lateral position error  $e_i^y$  and heading angle error  $e_i^\varphi$  are minimized:

$$\begin{cases}
 \min |e_i^y|^2 \\
 \min |e_i^\varphi|^2 
\end{cases}$$
(14)

#### 4. Controller design

In this section, the task of reducing fuel consumption, and safety of truck platoons are split into two layers. To provide a clear overview of the proposed methodology, the overall framework of the truck platoon control strategy is illustrated in Fig. 8. The framework adopts a hierarchical scheme that integrates DL-MPC. As shown in the figure, the upper layer is responsible for speed planning of the leading truck, while the lower layer employs distributed controllers for each following truck to ensure safety. The actor–critic networks are embedded in the DL-MPC scheme to enhance prediction and control efficiency, thereby improving both fuel economy and platoon stability.

#### 4.1. Speed planning of the leading truck

Considering the following capability of the following trucks, the speed planning of the leading truck is carried out, and the following trucks follow the speed of the leading truck to achieve the purpose of fuel saving. The position and speed of the truck are expressed as  $x = [s, v]^T$ , and the power of the engine is selected as the control input

Define the output as:

$$y = [s, v]^T \tag{15}$$

Denote the sampling time as  $\Delta T$ , the discrete form of (5) can be expressed as follows:

$$\begin{cases} x(h+1) = g(x(h), u(h)) \\ y(h) = x(h) \end{cases}$$

$$(16)$$

The control sequence in the prediction horizon is defined as:

$$U(h) = \{u(h|h), \dots, u(h+H-1|h)\}$$
(17)

where H is the prediction horizon within the speed planning layer, and note that h + j | h denotes the predicted value of the time instant h for the time instant h + j.

To determine the optimal economic speed for the leading truck, problem 1 need to be solved, which aims to find the speed that minimizes fuel consumption. The description of problem 1 is as follows:

## Problem 1.

$$\underset{U(h)}{\operatorname{minimize}} J = \sum_{h=0}^{H-1} E_{fuel}\left(x\left(h\right), u\left(h\right)\right) \tag{18a}$$

s.t

$$x(h+j+1|h) = g(x(h+j|h), u(h+j|h))$$
(18b)

$$y(h+j|h) = x(h+j|h)$$
(18c)

$$y(h|h) = y(h) \tag{18d}$$

$$F_{e,\min} \le F_e \le F_{e,\max} \tag{18e}$$

$$v_{\min} \le v \le v_{\max} \tag{18f}$$

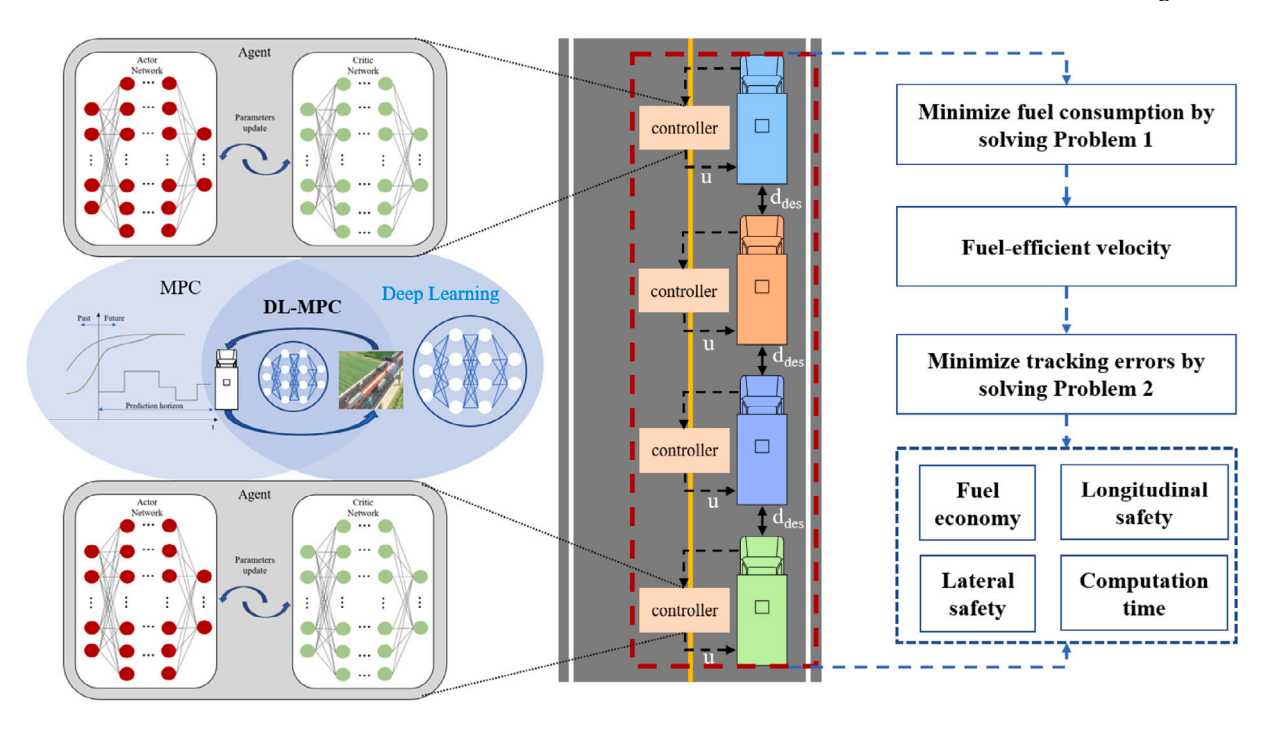


Fig. 8. Framework of the truck platoon control strategy.

In Problem 1, (18e) is the control constraint, (18f) represents the speed constraint of the highway. Note that in the speed planning layer, the formulation primarily focuses on the longitudinal dynamics and physical constraints of the truck, without explicitly modeling internal and external uncertainties. This modeling choice is consistent with many existing studies on fuel-efficient speed planning for truck platoons [3,8], where simplified longitudinal models are commonly adopted to ensure tractability of the optimization problem. By concentrating on the dominant dynamics and physical limitations of the truck, the speed planning problem can be effectively solved as an upperlevel optimization that generates a feasible and fuel-efficient reference trajectory for the platoon. Importantly, by first addressing the dominant dynamics under simplified conditions, this formulation provides a structured foundation for extending the method to more realistic scenarios, including mixed traffic, traffic signals, and uncertainties in vehicle dynamics. By concentrating on the dominant dynamics and physical limitations of the truck, the speed planning problem can be effectively solved as an upper-level optimization that generates a feasible and fuel-efficient reference trajectory for the platoon.

**Remark 3.** Problem 1 focuses on the speed planning of the leading truck, considering the tracking capabilities of the following trucks by applying control constraints. This is a reasonable approach given that it is neither efficient nor practical to plan different reference velocities for each truck. Although tracking the leading truck's reference speed may slightly increase fuel consumption, the gains in collaborative control and stability for the platoon outweigh this drawback.

#### 4.2. Platoon control based on DMPC

To ensure practical feasibility in controller design, the following assumptions are introduced prior to formulating the DMPC problem:

- The communication network among trucks is reliable and free of packet loss or delay, so that each truck can access the necessary state information from its neighbors in real time.
- The road geometry is known and detectable by onboard sensors, and all trucks are assumed to travel on the same lane.

Under the DMPC framework, each truck is equipped with an individual control unit.

Denote the state:

$$x_i = [v_i^x \quad v_i^y \quad \phi_i \quad \omega_i^f \quad \omega_i^r \quad e_i^p \quad e_i^y \quad e_i^q]^T \tag{19}$$

and the output:

$$y_{i} = [v_{i}^{x} e_{i}^{p} e_{i}^{y} e_{i}^{\varphi}]^{T}$$
(20)

The control inputs are the driving/brake torque of rear tires, and the steering angle of the front tires, respectively:

$$u_i = [T_i^d \ \delta_i]^T \tag{21}$$

Denote the sampling time as  $T_s$ . The discrete form of (11) can be expressed as follows:

$$\begin{cases} x_i(k+1) = f_i(x_i(k), u_i(k)) \\ y_i(k) = C_i x_i(k) \end{cases}$$
 (22)

where  $C_i = diag(1, 0, 0, 0, 0, 1, 1, 1), i = 0, 1, ..., N - 1$ .

Based on (22), the output of the *i*th truck is:

$$y_{i,des}(k) = \begin{bmatrix} v_{i,des}^{x}(k) & e_{i,des}^{p}(k) & e_{i,des}^{y}(k) & e_{i,des}^{\varphi}(k) \end{bmatrix}^{T}$$
 (23)

where  $v_{i,des}^x(k)$  is the desired longitudinal speed of the *i*th truck, and set  $v_{i,des}^x(k) = v_0(k)$ . Terms of  $e_{i,des}^p(k)$ ,  $e_{i,des}^y(k)$  and  $e_{i,des}^\varphi(k)$  represent the longitudinal expected position error, lateral expected position error and expected heading angle error of the *i*th truck, respectively.

For each truck i, The tracking error is defined as:

$$e_i(k) = y_i(k) - y_{i,des}(k)$$
 (24)

The control sequence in the prediction horizon is defined as:

$$U_i(k) = \{U_i(k|k), \dots U_i(k+N_p-1|k)\}$$
(25)

where  $N_p$  represents the prediction horizon within the platoon control layer. Note that k+j|k denotes the predicted value of the time instant k for the time instant k+j.

The objective of problem 2 is to ensure the safe control of trucks, allowing the trucks to maintain a platoon. The description of problem 2 is as follows:

#### Problem 2.

$$\underset{U_{i}(k)}{\operatorname{minimize}} J_{i}\left(e_{i}(k), U_{i}\left(k\right)\right) \tag{26a}$$

c f

$$x_i(k+j+1|k) = f_i(x_i(k+j|k), u_i(k+j|k))$$
 (26b)

$$y_i(k+j|k) = C_i x_i(k+j|k)$$
 (26c)

$$y_i(k|k) = y_i(k) \tag{26d}$$

$$T_{i,\min}^d \le T_i^d(k+j|k) \le T_{i,\max}^d \tag{26e}$$

$$\delta_{i,min} \le \delta_i(k+j|k) \le \delta_{i,max} \tag{26f}$$

$$e_i\left(k+N_n|k\right)=0\tag{26g}$$

where

$$J_{i}\left(e_{i}(k), U_{i}(k)\right) = \sum_{i=0}^{N_{p}-1} \left(\left\|e_{i}(k+j|k)\right\|_{Q_{i}}^{2} + \left\|u_{i}(k+j|k)\right\|_{R_{i}}^{2}\right)$$
(27)

In the objective function  $J_i$ , terms of  $Q_i$  and  $R_i$  are the weight matrices, (26e) and (26f) are the control constraints. Term of (26g) denotes the terminal equality constraint, which guarantees the asymptotic consensus of the truck platoon [62,63]. However, the terminal equality constraint in the actual solution is difficult to be satisfied. Here, term of (26g) is reformulated as a soft constraint to facilitate further processing, and the term of  $F_i\left(e_i\left(k+N_p|k\right)\right)$  is the terminal cost function. The expression of the terminal cost function is  $F_i\left(e_i\left(k+N_p|k\right)\right) = \left\|e_i\left(k+N_p|k\right)\right\|_{P_i}^2$ , where  $P_i$  is the terminal penalty matrix, with  $P_i = 10Q_i$ . Then, (27) can be rewritten as:

$$J_{i}\left(e_{i}(k), U_{i}(k)\right) = \sum_{j=0}^{N_{p}-1} \left(\left\|e_{i}(k+j|k)\right\|_{Q_{i}}^{2} + \left\|u_{i}(k+j|k)\right\|_{R_{i}}^{2}\right) + F_{i}\left(e_{i}(k+N_{p}|k)\right)$$
(28)

In summary, the objective of the DMPC formulation is to minimize spacing, velocity, and lateral errors while penalizing control efforts, thereby ensuring platoon consistency and meeting the control objectives. The constraints (26e)–(26f) reflect the actuator limitations of trucks, and the terminal condition (26g) is relaxed into a soft constraint with a terminal cost. The formulation relies on the assumptions of reliable communication, accurate local dynamics within the prediction horizon, and known road geometry. Such a distributed structure reduces computational burden and ensures scalability to larger platoons.

#### 4.3. Distributed learning-model predictive control

Reinforcement learning can be employed to learn solutions for specified optimal control problems in real-time [64]. Predictive controllers designed for nonlinear systems often involve solving non-convex constrained optimization problems. As the system state and control dimensions increase, the computational burden and data storage requirements also rapidly grow. Currently, numerical solutions are often obtained through iterative methods, and policy iteration techniques are effective means for solving optimal control strategies [65]. Here, the actor-critic neural network structure based on the policy iteration concept in RL is employed to solve the constrained optimization problem for each truck.

**Remark 4.** As a practical and efficient implementation of the DL-MPC method, neural networks and kernel-based basis vectors will be employed in the DL-MPC method.

Denote the stage cost function as:

$$r_i\left(e_i(k+j|k), u_i(k+j|k)\right) = \|e_i(k+j|k)\|_{Q_i}^2 + \|u_i(k+j|k)\|_{R_i}^2$$
 (29)

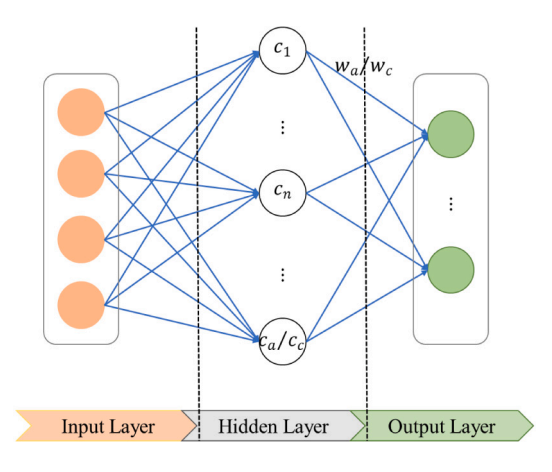


Fig. 9. Diagram of RBF neural network.

In the prediction horizon  $j \in [k, k + N_p - 1]$ , according to the Bellman optimality principle, the optimal cost function of the system satisfies [66,67]:

$$J_{i}^{*}\left(e_{i}\left(k+j|k\right)\right) = \min_{\|\bar{U}^{-1}u_{i}\|_{\infty} \le 1} \left(\begin{array}{c} r\left(e_{i}\left(k+j|k\right), u_{i}\left(k+j|k\right)\right) \\ +J_{i}^{*}\left(e_{i}\left(k+j+1|k\right)\right) \end{array}\right)$$
(30)

and 
$$J_i^*\left(e_i\left(k+N_p|k\right)\right) = \left\|e_i\left(k+N_p|k\right)\right\|_{P_i}^2$$
 when  $j=k+N_p$ .

Then, the optimal control  $u_i^* \left( e_i(k+j|k) \right)$  satisfies [66,67]:

$$u_{i}^{*}\left(e_{i}\left(k+j|k\right)\right) = \arg\min_{\left\|\bar{U}^{-1}u_{i}\right\|_{\infty} \leq 1} \left(\begin{array}{c} r_{i}\left(e_{i}\left(k+j|k\right), u_{i}\left(k+j|k\right)\right) \\ +J_{i}^{*}\left(e_{i}\left(k+j+1|k\right)\right) \end{array}\right)$$
(31)

where  $\bar{U}$  is the control constraint matrix and  $\bar{U} = \operatorname{diag}\left\{T_{i,\max}^d, \delta_{i,\max}\right\}$ .

Set the number of iterations as l, the convergence accuracy as  $\varepsilon$ , and the maximum number of iterations as  $l_{\text{max}}$ . For problem 2, the steps of iterative DL-MPC method are summarized in Algorithm 1 [67].

# Algorithm 1 Iterative DL-MPC method

```
Initialize: l = 0, set \varepsilon > 0 and J_i^0\left(e_i(k+j|k)\right) = 0, \ j \in [k,k+N_p-1]; repeat for all j = k, k+1, \cdots k+N_p-1 do Calculate u_i^l\left(e_i(k+j|k)\right) via (31); Generate the next state e_i(k+j+1|k) via (22); Calculate J_i^{l+1}\left(e_i(k+j|k)\right) by using J_i^{l+1}\left(e_i(k+j|k)\right) = r\left(e_i(k+j|k), u_i(k+j|k)\right) + J_i^l\left(e_i(k+j+1|k)\right), j \in [k,k+N_p-1]; end for until \|J_i^{l+1}\left(e_i(k+j|k)\right) - J_i^l\left(e_i(k+j|k)\right)\| < \varepsilon or l = l_{\max}.
```

In the DL-MPC method, the actor network is used to approximate the optimal control law  $u_i^*(k+j|k)$ , and the critic networks are used to approximate  $\lambda_i^*\left(e_i\left(k+j|k\right)\right)$ , where  $\lambda_i^*=\frac{\partial J_i^*}{\partial e_i}$ , which represents the derivative of the optimal cost function  $J_i^*$  with respect to  $e_i$ . In the prediction horizon  $j\in[k,k+N_p-1]$ ,  $N_p$  actor neural networks and  $N_p$  critic neural networks will be need to approximate  $u_i^*\left(k+j|k\right)$  and  $\lambda_i^*\left(e_i\left(k+j|k\right)\right)$  at each step in the prediction horizon, respectively. In this paper, a radial basis function (RBF) neural network structure is adopted to realize actor networks and critic networks [68] and its diagram is shown in Fig. 9.

For  $j \in [k, k + N_p - 1]$ , each actor network is designed as:

$$\hat{u}_{i}^{l}\left(e_{i}(k+j|k)\right) = \bar{U}\Gamma\left(\sum_{m=1}^{c_{a}}w_{a,l}^{[m]}(k+j|k)\,\varphi^{[m]}\left(e_{i}(k+j|k)\right)\right)$$

$$= \bar{U}\Gamma\left(W_{a,l}(k+j|k)^{T}\Psi\left(e_{i}(k+j|k)\right)\right)$$
(32)

and each critic network is designed as:

$$\hat{\lambda}_{i}^{l}\left(e_{i}(k+j|k)\right) = \sum_{m=1}^{c_{c}} w_{c,l}^{[m]}(k+j|k)\phi^{[m]}\left(e_{i}(k+j|k)\right)$$

$$= W_{c,l}(k+j|k)^{T} \Phi\left(e_{i}(k+j|k)\right)$$
(33)

where  $\Gamma\left(\cdot\right)$  is  $\tanh\left(\cdot\right)$  and  $\|\tanh\left(\cdot\right)\|\leq 1$ . Terms of  $c_a$  and  $c_c$  are the number of the center points of the hidden layer of the actor networks and the critic networks, respectively. Terms of  $w_{a,l}^{[m]}\left(k+j|k\right)$  and  $w_{c,l}^{[m]}\left(k+j|k\right)$  are the weight vectors between the mth center point and the output layer of the jth actor networks and critic networks when the number of iterations is l, respectively, and  $w_{a,l}^{[m]}\left(k+j|k\right)\in\mathbb{R}^2$ ,  $w_{c,l}^{[m]}\left(k+j|k\right)\in\mathbb{R}^4$ . Terms of  $\varphi^{[m]}\left(e_i\left(k+j|k\right)\right)$  and  $\varphi^{[m]}\left(e_i\left(k+j|k\right)\right)$  represent the activation function of the mth center point in the hidden layer of the actor networks and the critic networks, respectively. Terms of  $W_{a,l}\left(k+j|k\right)$  and  $W_{c,l}\left(k+j|k\right)$  denote the weight matrices of the jth actor networks and critic networks, respectively. Terms of  $\Psi\left(e_i\left(k+j|k\right)\right)$  and  $\Phi\left(e_i\left(k+j|k\right)\right)$  are the basis vectors in the actor networks and the critic networks, respectively, and they can be denoted as follows:

$$\begin{cases}
\Psi\left(e_{i}(k+j|k)\right) = \left(\exp^{-\left\|e_{i}-e_{i}^{k}\right\|^{2}/\kappa^{2}}; \cdots \exp^{-\left\|e_{i}-e_{i}^{c_{a}}\right\|^{2}/\kappa^{2}}\right) \\
\Phi\left(e_{i}(k+j|k)\right) = \left(\exp^{-\left\|e_{i}-e_{i}^{k}\right\|^{2}/\kappa^{2}}; \cdots \exp^{-\left\|e_{i}-e_{i}^{c_{a}}\right\|^{2}/\kappa^{2}}\right)
\end{cases} (34)$$

where  $(e_i^1 \cdots e_i^{c_a})$  and  $(e_i^1 \cdots e_i^{c_c})$  are used to denote the hidden layer centroids of the actor networks and the critic networks, respectively, and  $\kappa = 1.1$ ,  $c_a = c_c = 5$ .

The optimal control law  $u_i^*(k+j|k)$  satisfies:

$$\frac{\partial J_i^* \left( e_i \left( k + j | k \right) \right)}{\partial u_i^* \left( k + j | k \right)} = 0 \tag{35}$$

Combining (29), (30) and (35):

$$u_{i}^{*}(k+j|k) = -\frac{1}{2R_{i}} \left( \frac{\partial e_{i}(k+j+1|k)}{\partial u_{i}^{*}(k+j|k)} \right)^{T} \lambda_{i}^{*} \left( e_{i}(k+j+1|k) \right)$$
(36)

Let the right side of (32) and (36) be equal, the weight updating of the actor networks can be obtained as follows:

$$W_{a,l}^{p+1}(k+j|k) = \left(\Psi\left(e_{i}\left(k+j|k\right)\right)\Psi^{T}\left(e_{i}\left(k+j|k\right)\right)^{T}\right)^{-1} \times \Psi\left(e_{i}\left(k+j|k\right)\right)$$

$$\times \left(\Gamma^{-1}\left[\bar{U}^{-1}\left(\frac{-\frac{1}{2R_{l}}\left(\frac{\partial e_{i}(k+j+1|k)}{\partial \hat{q}_{i}^{l,p}\left(e_{i}(k+j|k)\right)}\right)^{T}}{\times W_{c,l}(k+j+1|k)}\right)^{T}\right)\right)^{T}$$

$$\times \Psi\left(e_{i}\left(k+j+1|k\right)\right)$$

$$\times \Phi\left(e_{i}\left(k+j+1|k\right)\right)$$
(37)

where  $W_{a,l}^{p+1}(k+j|k)$  denotes the weight matrix of the jth actor network at the lth policy evaluation and the pth policy update, and  $W_{c,l}(k+j|k)$  denotes the weight matrix of the jth critic network at the lth policy evaluation.  $\hat{u}_i^{l,p}\left(e_i(k+j|k)\right)$  denotes the output of the jth actor network during the lth policy evaluation and the pth policy update.

Note that when updating the weight of the jth actor network, the output of the (j+1)th critic network is need to be used. When  $j=k+N_p-1$ , the weight updating of the  $(k+N_p-1)$ th actor network is as follows:

$$\begin{split} W_{a,l}^{p+1}\left(k+j|k\right) = & \left( \Psi\left(e_i\left(k+j|k\right)\right) \Psi\left(e_i\left(k+j|k\right)\right)^T\right)^{-1} \times \Psi\left(e_i\left(k+j|k\right)\right) \\ \times & \left( \Gamma^{-1} \left( \frac{1}{2R_i} \left( \frac{\partial e_i(k+j+1|k)}{\partial \hat{u}_i^{l,p}(e_i(k+j|k))} \right)^T \right) \right) \right)^T \\ \times & 2P_i e_i\left(k+j+1|k\right) \end{split}$$

By taking the derivative of (30) with respect to  $u_i^*(k+j|k)$ :

$$\frac{\partial \left(r_{i}\left(e_{i}\left(k+j|k\right), u_{i}^{*}\left(k+j|k\right)\right) + J_{i}^{*}\left(e_{i}\left(k+j+1|k\right)\right)\right)}{\partial u_{i}^{*}\left(k+j|k\right)} \\
= \frac{\partial r_{i}\left(e_{i}\left(k+j|k\right), u_{i}^{*}\left(k+j|k\right)\right)}{\partial u_{i}^{*}\left(k+j|k\right)} + \left(\frac{\partial e_{i}\left(k+j+1|k\right)}{\partial u_{i}^{*}\left(k+j|k\right)}\right)^{T} \\
\times \frac{\partial J_{i}^{*}\left(e_{i}\left(k+j+1|k\right)\right)}{\partial e_{i}\left(k+j+1|k\right)} \tag{39}$$

By taking the derivative of (30) with respect to  $e_i(k+j|k)$ :

$$\begin{split} \lambda_{i}^{*}\left(e_{i}\left(k+j|k\right)\right) &= \frac{\partial\left(r_{i}\left(e_{i}\left(k+j|k\right),u_{i}^{*}\left(k+j|k\right)\right) + J_{i}^{*}\left(e_{i}\left(k+j+1|k\right)\right)\right)}{\partial e_{i}\left(k+j|k\right)} \\ &= \frac{\partial r_{i}\left(e_{i}\left(k+j|k\right),u_{i}^{*}\left(k+j|k\right)\right)}{\partial e_{i}\left(k+j|k\right)} \\ &+ \left(\frac{\partial u_{i}^{*}\left(k+j|k\right)}{\partial e_{i}\left(k+j|k\right)}\right)^{T} \frac{\partial r_{i}\left(e_{i}\left(k+j|k\right),u_{i}^{*}\left(k+j|k\right)\right)}{\partial u_{i}^{*}\left(k+j|k\right)} \\ &+ \left(\frac{\partial u_{i}^{*}\left(k+j|k\right)}{\partial e_{i}\left(k+j|k\right)}\right)^{T} \left(\frac{\partial e_{i}\left(k+j+1|k\right)}{\partial u_{i}^{*}\left(k+j|k\right)}\right)^{T} \\ &\times \frac{\partial J_{i}^{*}\left(e_{i}\left(k+j+1|k\right)\right)}{\partial e_{i}\left(k+j+1|k\right)} \\ &+ \left(\frac{\partial e_{i}\left(k+j+1|k\right)}{\partial e_{i}\left(k+j+1|k\right)}\right)^{T} \frac{\partial J_{i}^{*}\left(e_{i}\left(k+j+1|k\right)\right)}{\partial e_{i}\left(k+j+1|k\right)} \end{split}$$

$$(40)$$

Combining (39) and (40):

$$\begin{split} \lambda_{i}^{*}\left(e_{i}\left(k+j|k\right)\right) &= \frac{\partial r_{i}\left(e_{i}\left(k+j|k\right), u_{i}^{*}\left(k+j|k\right)\right)}{\partial e_{i}\left(k+j|k\right)} \\ &+ \left(\frac{\partial e_{i}\left(k+j+1|k\right)}{\partial e_{i}\left(k+j|k\right)}\right)^{T} \frac{\partial J_{i}^{*}\left(e_{i}\left(k+j+1|k\right)\right)}{\partial e_{i}\left(k+j+1|k\right)} \\ &= 2Q_{i}e_{i}\left(k+j|k\right) \\ &+ \left(\frac{\partial e_{i}\left(k+j+1|k\right)}{\partial e_{i}\left(k+j|k\right)}\right)^{T} \lambda_{i}^{*}\left(e_{i}\left(k+j+1|k\right)\right) \end{split} \tag{41}$$

Let the right side of (33) and (41) be equal, the weight updating of the critic networks can be obtained as follows:

$$W_{c,l+1}(k+j|k) = \left(\boldsymbol{\Phi}\left(e_{i}(k+j|k)\right)\boldsymbol{\Phi}\left(e_{i}(k+j|k)\right)^{T}\right)^{-1}\boldsymbol{\Phi}\left(e_{i}(k+j|k)\right)$$

$$\times \begin{pmatrix} 2Q_{i}e_{i}(k+j|k) + \left(\frac{\partial e_{i}(k+j+1|k)}{\partial e_{i}(k+j|k)}\right)^{T} \\ \times W_{c,l}(k+j+1|k)^{T}\boldsymbol{\Phi}\left(e_{i}(k+j+1|k)\right) \end{pmatrix}^{T}$$

$$(42)$$

where  $W_{c,l+1}(k+j|k)$  is the weight matrix of the jth critic network at the (l+1)th policy evaluation.

When  $j = k + N_p - 1$ , the weight updating of the  $(k + N_p - 1)$ th critic network is as follows:

$$W_{c,l+1}(j) = \left(\boldsymbol{\Phi}\left(e_i(k+j|k)\right)\boldsymbol{\Phi}\left(e_i(k+j|k)\right)^T\right)^{-1}\boldsymbol{\Phi}\left(e_i(k+j|k)\right) \times \left(\begin{array}{c} 2Q_ie_i(k+j|k) + \left(\frac{\partial e_i(k+j+1|k)}{\partial e_i(k+j|k)}\right)^T \\ \times 2P_ie_i(k+j+1|k) \end{array}\right)^T$$

$$(43)$$

Then, the main procedures in iterative DL-MPC algorithm based on neural network are given in Algorithm 2.

**Remark 5.** The convergence of the iterative DL-MPC algorithm is guaranteed, i,e., when the number of iterations  $l \to \infty$ , satisfying  $u_i^l \to u_i^*$ ,  $J_i^l \to J_i^*$  and  $\lambda_i^l \to \lambda_i^*$  [66,69]. Due to the limitation of calculation time, the maximum number of iterations and convergence accuracy need to be specified in advance in this paper. Define  $l_{\rm max}$  as the maximum number of weight updates of critic network in each prediction horizon,  $p_{\rm max}$  as the maximum number of weight updates of actor network,  $\Delta W_a(\varepsilon)$  and  $\Delta W_c(\varepsilon)$  as the convergence thresholds of the weights of actor network and critic network, respectively.

(38)

### Algorithm 2 DL-MPC algorithm based on neural network

**Input:** The maximum iteration numbers  $l_{\max}$  and  $p_{\max}$ ; the convergence thresholds  $\Delta W_a\left(\varepsilon\right)$  and  $\Delta W_c\left(\varepsilon\right)$ ; truck status at the initial moment; **Output:** Optimal or sub-optimal control policy  $u_i^*\left(k|k\right)$ .

1: Initialize the weight matrix of actor networks and critic networks, and set *l* = 0;

```
2: repeat
3:
       for all j = k, k + 1, \dots k + N_n - 1 do
4:
          p = 0;
          repeat
5:
             Calculate \hat{u}_{i}^{l}\left(e_{i}\left(k+j|k\right)\right) via (32);
6:
7:
             Calculate e_i(k+j+1|k) via (22);
             Update the actor weights via (37) and (38);
8:
9:
             Set p = p + 1.
          until p = p_{\text{max}} or \left\| W_{a,l}^{p+1}(k+j|k) - W_{a,l}^{p}(j) \right\| \le \Delta W_a(\varepsilon);
10:
          Calculate \hat{u}_i^l(e_i(k+j|k)) via (32);
11:
          Calculate e_i(k+j+1|k) via (22);
12:
          Update the critic weights via (42) and (43).
13:
14:
       end for
       return l = l + 1;
15:
16: until l = l_{\text{max}} or ||W_{c,l}(k+j|k) - W_{c,l-1}(k+j|k)|| \le \Delta W_c(\varepsilon);
17: Calculate u_i^*(k|k) via (31) and apply it to the system;
18: Set k = k + 1 and go back to 1.
```

Table 3
The parameters of trucks.

Parameters	Value	Parameters	Value
$C_{tf}$	0.003	$C_{aero}$	0.6
A	10	ρ	$1.29 \text{ (kg m}^{-3}\text{)}$
α	1	$I_z$	130421.8 (kg m <sup>2</sup> )
γ	44	a	3.5 (m)
β	737	b	1.5 (m)
ε	33	g	$9.8 \text{ m/s}^2$
τ	5	$J_f$	24 (kg m <sup>2</sup> )
$\eta_f$	0.9	$J_r^{'}$	48 (kg m <sup>2</sup> )
$\eta_c$	0.4	$R_{\rho}$	0.51 (m)

**Remark 6.** The parameters  $l_{\text{max}}$  and  $p_{\text{max}}$  are set to be constants and independent of the prediction horizon  $N_p$ .

**Remark 7.** The RBF networks are employed as the function approximators for the actor and critic networks within the iterative DL-MPC scheme. The networks are trained online over each prediction horizon, not with a fixed offline dataset. At time instant k, the training samples are the error vectors  $\left\{e_i\left(k+j|k\right)\right\}_{j=0}^{N_p-1}$  generated by the system dynamics (22) under the current policy, and the actor and critic weights are updated by the policy-iteration-based rules in (37)–(38) and (42)–(43), respectively. The RBF basis vectors  $\Psi\left(\cdot\right)$  and  $\Phi\left(\cdot\right)$  use Gaussian kernels and shape parameter  $\kappa=1.1$ . Terms of  $c_a=c_c=5$  are set and the centers are kept fixed during online updates (Fig. 9, (32)–(34)). Convergence is determined by the preset iteration limits  $l_{\max}$ ,  $p_{\max}$ , as well as the thresholds on weight changes in Algorithm 2.

#### 5. Simulation and analysis

This section provides a simulation study on the fuel-saving control and computation time of the controller. A truck platoon consists of one leading truck and three following trucks. The parameters of trucks are shown in Table 3. The parameters of the controllers are shown in Table 4 and the tire parameters are shown in Table 5.

### 5.1. Speed optimization of the leading truck

Scenario 1 of slope road is shown in Fig. 10(a), which is composed of three parts, a flat stretch, an uphill stretch and a downhill stretch with

**Table 4**The parameters of controllers.

Parameters	Value
$N_p$	3
$\hat{H}$	20
$\Delta T$	0.01 (s)
$T_s$	0.01 (s)
$Q_i$	$10^5 \times \text{diag}(5, 70, 50, 50)$
$R_i$	diag(0.06, $1.5 \times 10^6$ )
$d_{des}$	16 (m)
$\Gamma()$	tanh(x)
$l_{\text{max}}$	4
$p_{\rm max}$	4
$\Delta W_a(\epsilon)$	$10^{-2}$
$\Delta W_{c}\left( \varepsilon \right)$	$10^{-2}$

**Table 5**The Tire parameters.

Tire forces	В	С	D	E
$F_i^{xf}$	8.61	1.58	22 053	0.5624
$F_i^{xr}$	8.61	1.58	44 625	0.5624
$F_i^{yf}$	6.59	1.58	22 503	-0.3028
$F_i^{yr}$	6.59	1.58	44 625	-0.3028

 $3^{\circ}$  and  $-3^{\circ}$ , respectively. The curvature information is shown in Fig. 10(b), where the curvature is 0.0025. In this paper, the road adhesion coefficient is 0.85.

Scenario 2 of slope road is shown in Fig. 11(a), which is composed of three parts, a flat stretch, a downhill stretch and an uphill stretch with  $-2^{\circ}$  and  $2^{\circ}$ , respectively. The curvature information is shown in Fig. 11(b), where the curvature is 0.002.

The profiles of the fuel-efficient velocity of the leading truck in two scenarios are shown in Fig. 10(c) and Fig. 11(c), respectively. The road speed limit  $v_{\rm min}$  and  $v_{\rm max}$  are 72 km/h and 90 km/h. It can be seen from Fig. 10(c) and Fig. 11(c) that the truck velocity does not exceed the speed limit under this road condition and meets the requirements of road speed limit.

## 5.2. Platoon control

#### 5.2.1. Scenario 1

The initial longitudinal velocity of leading truck is  $22 \, \text{m/s}$ , the initial longitudinal velocities of the following trucks are  $21 \, \text{m/s}$ . Set the initial longitudinal spacing errors of the following trucks as  $-1 \, \text{m}$ ,  $-2 \, \text{m}$ ,  $-3 \, \text{m}$ , respectively. Both the initial lateral position errors and heading angular errors are  $0. \, \text{Fig.} \, 12(a)$  shows the driving paths of the truck platoon on the expressway in Scenario 1, where the three following trucks can travel along the desired trajectory. Fig. 12(b) shows the longitudinal positions of the platoon. As shown in Fig. 12(b), the trajectories of the four trucks remain distinct throughout the entire simulation, with no overlap or intersection. This indicates that no collisions occurred within the platoon, ensuring longitudinal safe operation during the simulation. Fig. 12(c) shows the longitudinal velocities of the platoon, which can be seen from Fig. 12(c) that when the road conditions change, the longitudinal velocities of the following trucks are quickly consistent with the longitudinal velocity of the leading truck.

Fig. 13 shows the simulation results based on the iterative DL-MPC method. In Fig. 13(a), the maximum longitudinal spacing error of the platoon fluctuates within  $\pm 0.7$  m, and finally tends to 0. Fig. 13(b) is the heading angle errors of the trucks, and the maximum deviation is not more than 0.025 rad, which meets the control requirements. Fig. 13(c) shows the lateral position errors of the following trucks, and the maximum error is about 0.09 m.

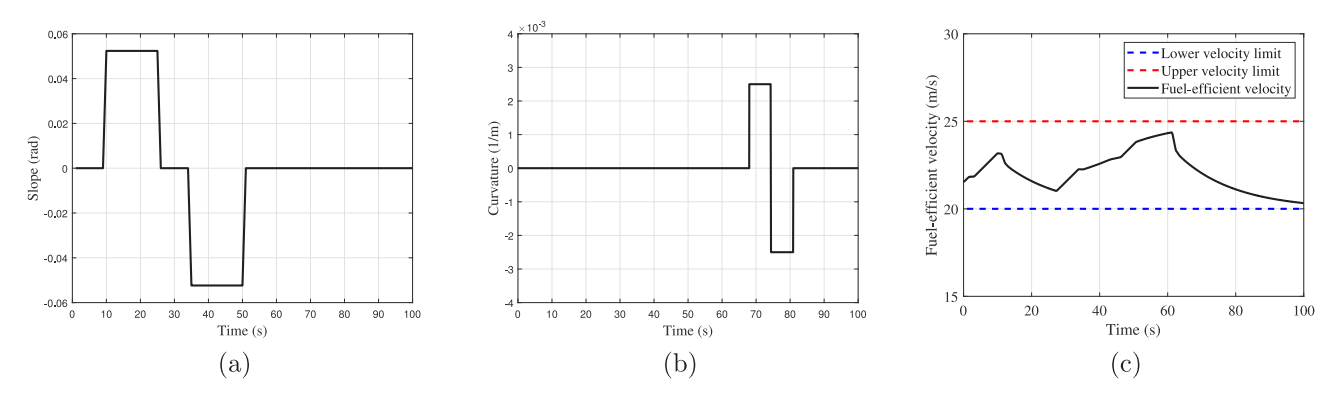


Fig. 10. Scenario 1: (a) scenario of slope road, (b) road curvature, (c) fuel-efficient velocity.

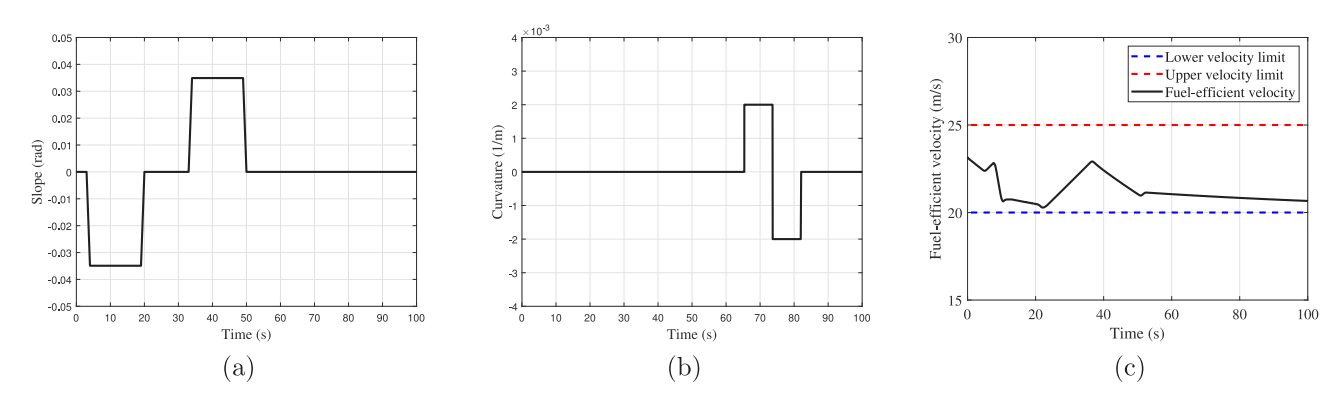


Fig. 11. Scenario 2: (a) scenario of slope road, (b) road curvature, (c) fuel-efficient velocity.

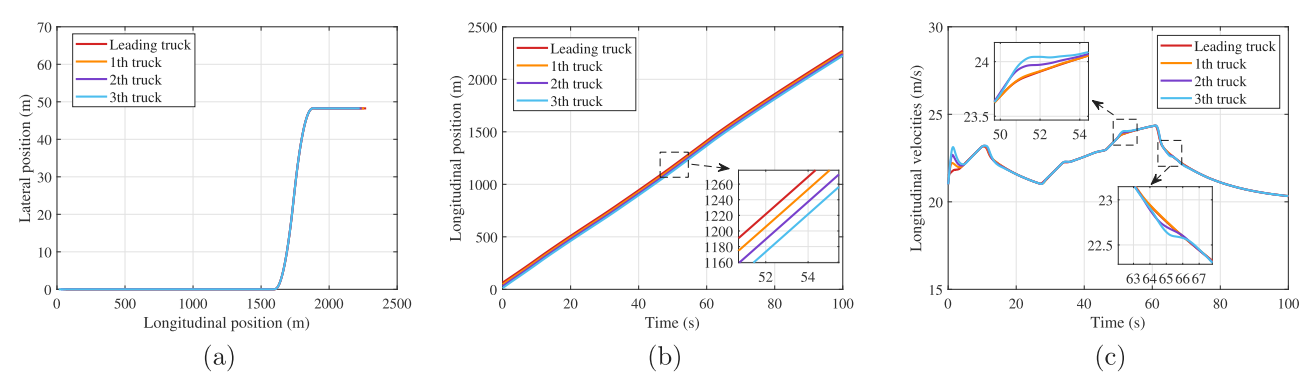


Fig. 12. DL-MPC in Scenario 1: (a) driving paths, (b) longitudinal position, (c) longitudinal velocities.

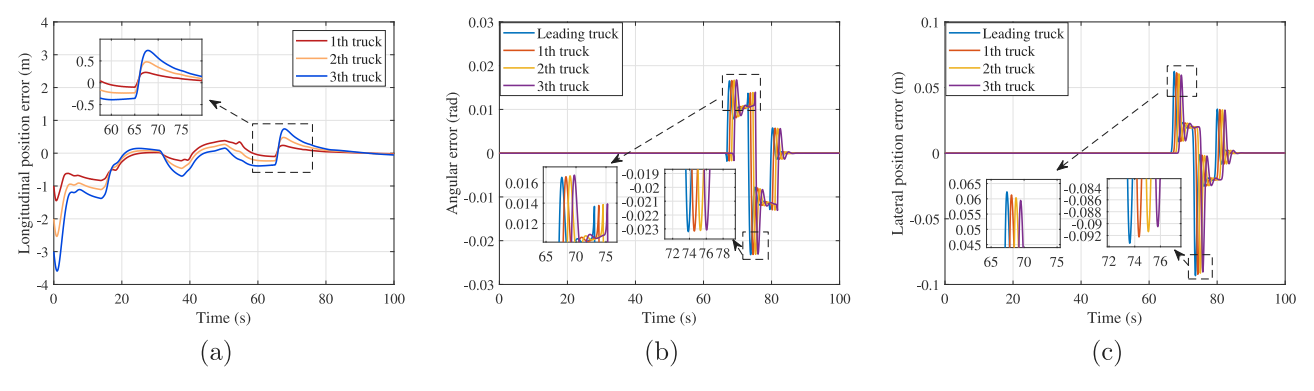


Fig. 13. DL-MPC in Scenario 1: (a) longitudinal spacing errors of following trucks, (b) angular errors of trucks, (c) lateral position errors of trucks.

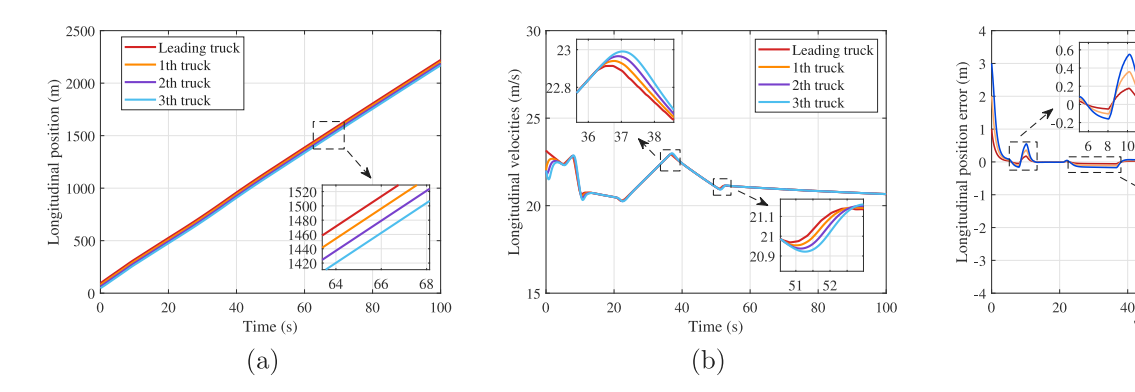


Fig. 14. DL-MPC in Scenario 2: (a) longitudinal position, (b) longitudinal velocities, (c) longitudinal spacing errors of following trucks.

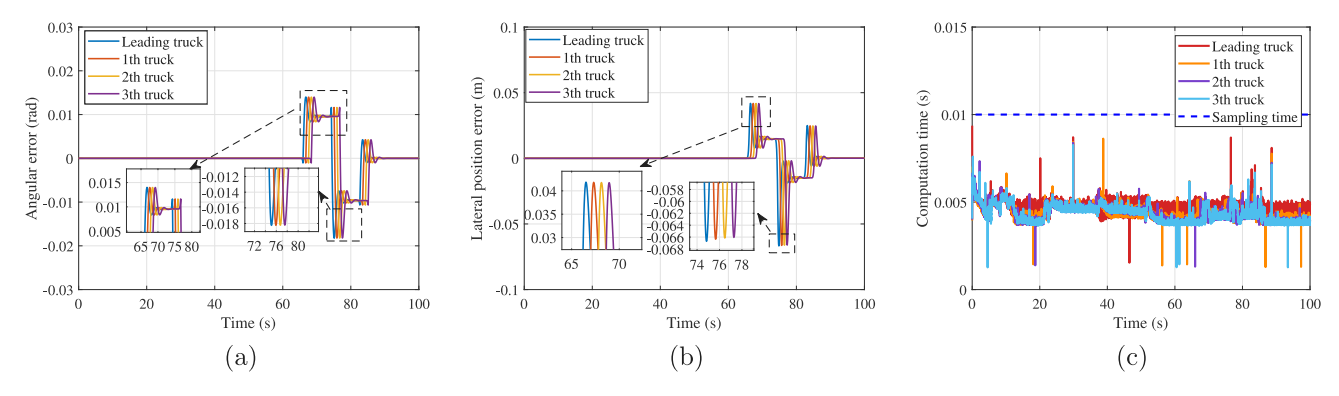


Fig. 15. DL-MPC in Scenario 2: (a) angular errors of trucks, (b) lateral position errors of trucks, (c) computation time.

## 5.2.2. Scenario 2

The initial longitudinal velocity of the leading truck is 23~m/s, the initial longitudinal velocities of the following trucks are 22~m/s. Set the initial longitudinal spacing errors of the following trucks as 1~m, 2~m, 3~m, respectively. Both the initial lateral position errors and heading angular errors are 0.

Fig. 14(a) shows the longitudinal positions of the platoon. As illustrated in Fig. 14(a), the trajectories of the four trucks remain distinct throughout the entire simulation, without any overlap or crossing. This indicates that no collisions occur within the platoon, thereby ensuring longitudinal safety. Fig. 14(b) shows the longitudinal velocities of the platoon. It can be observed from Fig. 14(b) that when the road conditions change, the longitudinal velocities of the following trucks quickly converge to that of the leading truck. In Fig. 14(c), the maximum longitudinal spacing error of the platoon fluctuates within ±0.6 m and eventually tends to zero. Fig. 15(a) presents the heading angle errors of the trucks, where the maximum deviation does not exceed 0.019 rad, satisfying the control requirements. Fig. 15(b) shows the lateral position errors of the following trucks, with a maximum error of about 0.07 m. From Fig. 15(c), it can be seen that the computation time remains less than the sampling time.

### 5.3. Comparison experiments

RL methods have been increasingly applied to truck platoon control problems in recent years, owing to their ability to optimize decision-making in complex environments. RL is particularly effective in handling high-dimensional state spaces and nonlinear system behaviors, making it well-suited for the challenges associated with coordinated control of multiple trucks. Therefore, to demonstrate the superior control performance of the proposed method, comparison experiments are conducted using the DMPC algorithm and the TD3 algorithm [70] in Scenario 1.

Fig. 16 shows the simulation results based on DMPC. As shown in Fig. 16(a), the longitudinal position error of the platoon is minimal,

indicating good longitudinal tracking performance. Figs. 16(b) and 16(c) illustrate the heading angle error and lateral position error of the platoon, respectively, further demonstrating the effective control performance of the DMPC algorithm.

1th truck

3th truck

100

-0.2

-0.4

Time (s)

(c)

28 30 32 34 36

In contrast, Fig. 17(a) presents the longitudinal spacing error under the TD3 algorithm. It can be observed that the follower trucks exhibit significant fluctuations in position error, which do not converge to zero. This suggests poor performance in longitudinal control. Figs. 17(b) and 17(c) show the heading angle error and lateral position error, respectively. While the heading angle error experiences minor oscillations at the initial stage and during curve negotiation, the lateral position error exhibits a more noticeable fluctuation of approximately 0.044 m at the beginning. Although the platoon does not encounter any critical safety issues during the simulation and both the heading angle and lateral position errors eventually converge to zero, the observed oscillations indicate potential safety risks, which are unacceptable in practical applications. It is worth noting that, unlike MPC, which explicitly incorporates system constraints into its optimization framework, RL lacks inherent mechanisms for constraint enforcement.

Fig. 18 shows the comparison of the control performance of the three methods. Fig. 18(a) illustrates the longitudinal spacing errors of the three following trucks under the three control algorithms. As shown in the figure, the DMPC algorithm yields the smallest longitudinal spacing errors across all trucks, indicating better tracking performance. In contrast, the TD3 algorithm results in significantly larger errors, particularly for the second following truck, whose maximum longitudinal deviation reaches approximately –6.1 m. Figs. 18(b) and 18(c) present the angular error and lateral position error of the first following truck as it enters the curve under the three control algorithms. As shown in Fig. 18(b), the DL-MPC and DMPC algorithms exhibit comparable performance, whereas the TD3 algorithm results in noticeably larger angular errors. In Fig. 18(c), although the TD3 algorithm appears to produce smaller lateral position errors, a comparison with Fig. 17(c)

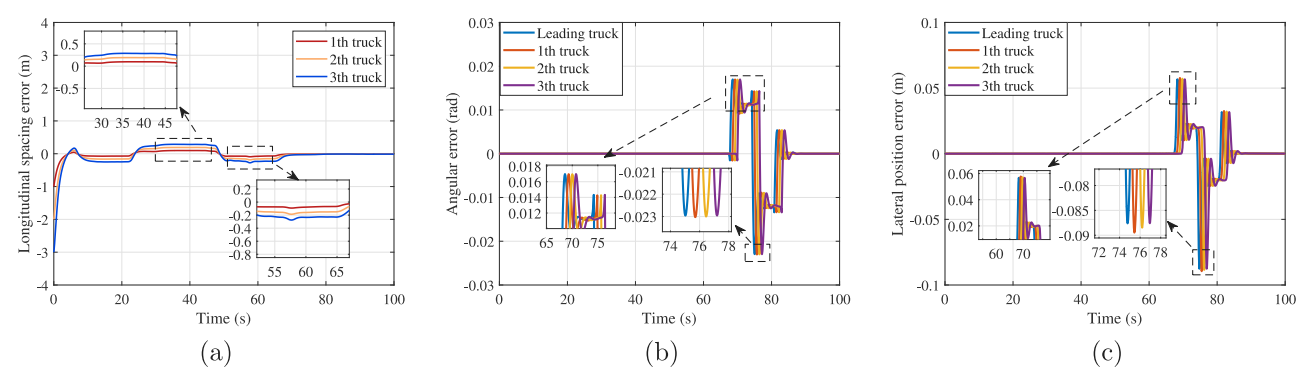


Fig. 16. DMPC: (a) longitudinal spacing errors of following trucks, (b) angular errors of trucks, (c) lateral position errors of trucks.

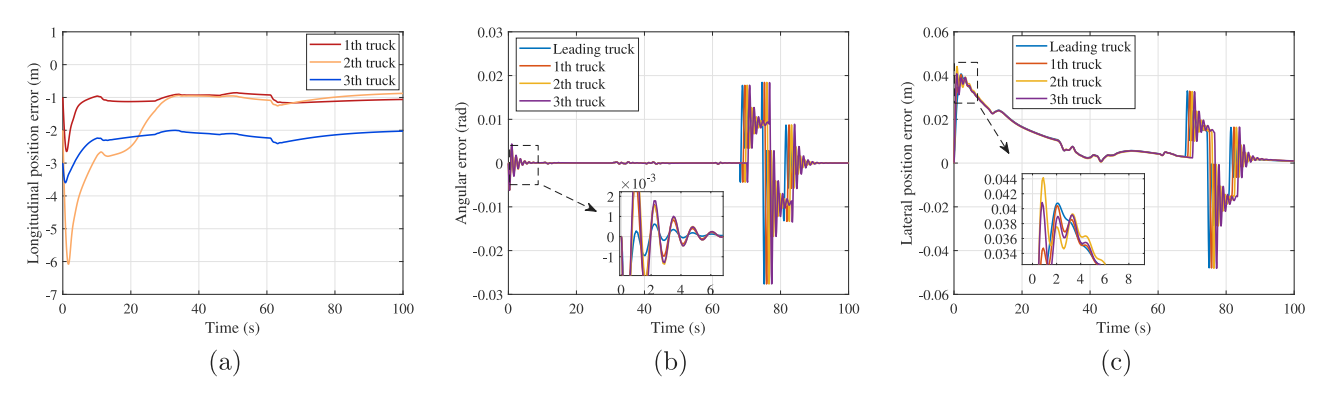


Fig. 17. TD3: (a) longitudinal spacing errors of following trucks, (b) angular errors of trucks, (c) lateral position errors of trucks.

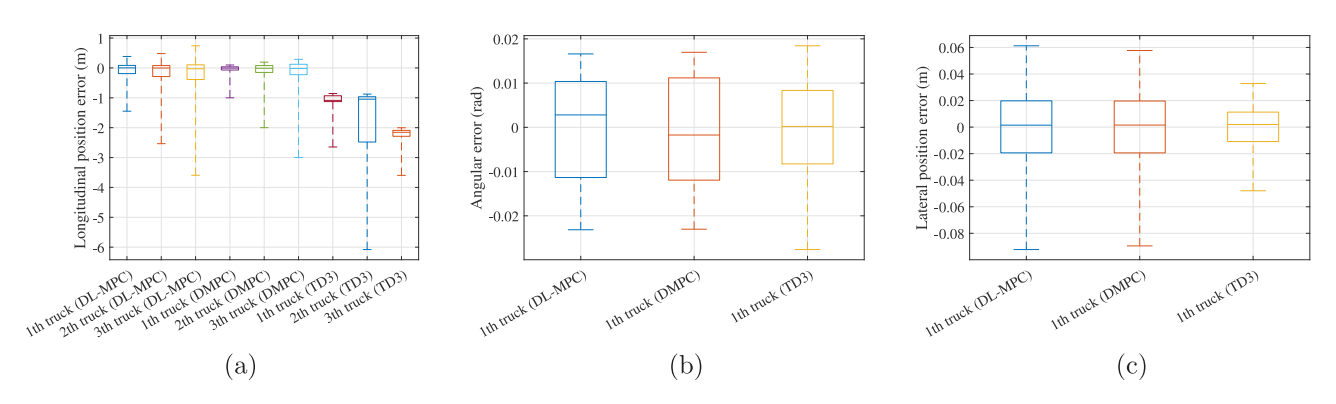


Fig. 18. Comparison of the control performance of the three methods: (a) longitudinal spacing errors of following trucks, (b) angular error of the 1th truck, (c) lateral position error of the 1th truck. (In the boxplot, the five values from the top to the bottom in a box denote the maximum, the third quartile, sample median, the first quartile, and the minimum value of the data set.).

reveals that the truck exhibits significant oscillations during the maneuver. These oscillations, despite the smaller error, may compromise the safety of the truck platoon.

Fig. 19 shows the computation time of the three methods. The values of three methods are shown in Table 6. It can be seen that the computation time of the DL-MPC algorithm is less than the sampling time  $T_s$ . The computation time of the DMPC algorithm is much larger than the sampling time. It is worth noting that the TD3 algorithm exhibits a significantly shorter computation time, primarily because it does not rely on solving optimization problems online. Instead, it utilizes a trained policy network to make rapid control decisions.

Therefore, by comparing the control performance and computation time across the three methods, the proposed method demonstrates superior overall performance, achieving a favorable balance between control performance and computational efficiency.

**Table 6**Comparison of the computation time of the three methods

comparison of the compatition time of the time methods.				
Methods	Minimum	Maximum	Average	
DL-MPC	1.1 (ms)	7 (ms)	1.45 (ms)	
DMPC	4.8 (ms)	332.3 (ms)	52.65 (ms)	
TD3	$4.7 \times 10^{-3}$ (ms)	$94 \times 10^{-3} \text{ (ms)}$	$8.23 \times 10^{-3} \text{ (ms)}$	

### 5.4. Fuel consumption of platoons

This part presents the fuel consumption for speed planning, constant speed, experience-based speed setting [31], and speed planning based on RL [34], respectively, to demonstrate the efficiency of the fuel-saving strategy in Scenario 1. Figs. 20 to 23 show the platoon control results under three different speed scenarios.

Fig. 20 shows the longitudinal velocities of the platoon under three different scenarios. From Fig. 20, it can be observed that as the

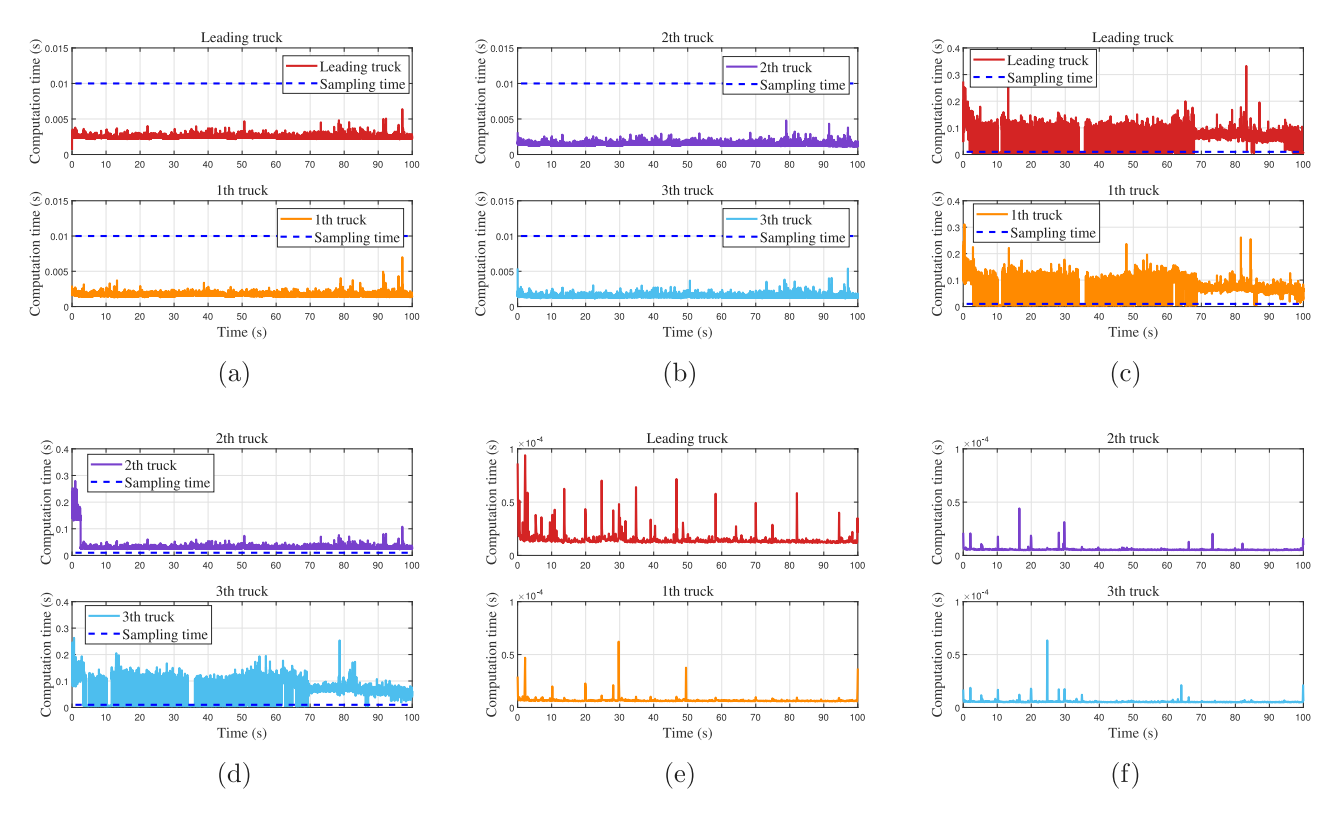


Fig. 19. Comparison of the computation time of the three methods: (a)–(b) computation time based on DL-MPC, (c)–(d) computation time based on DMPC, (e)–(f) computation time based on TD3.

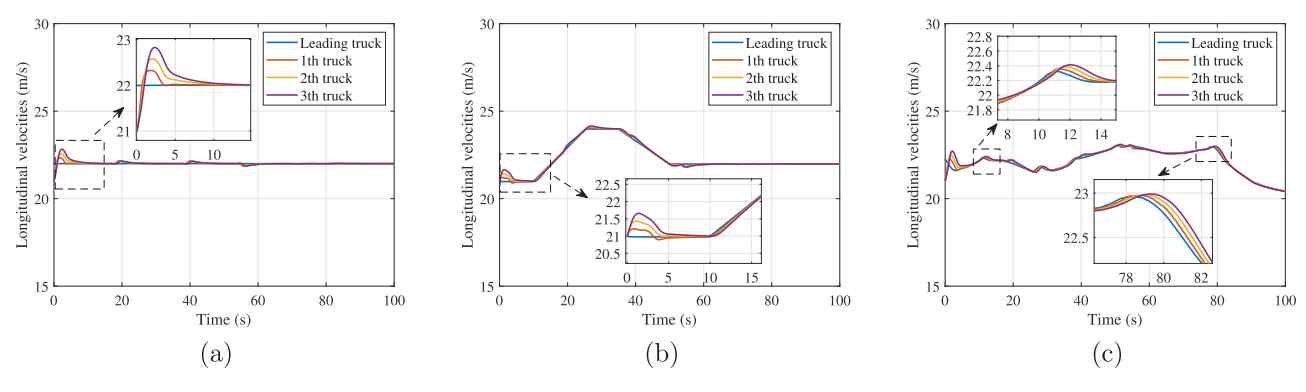


Fig. 20. Longitudinal velocities: (a) constant speed, (b) speed setting, (c) RL-speed planning.

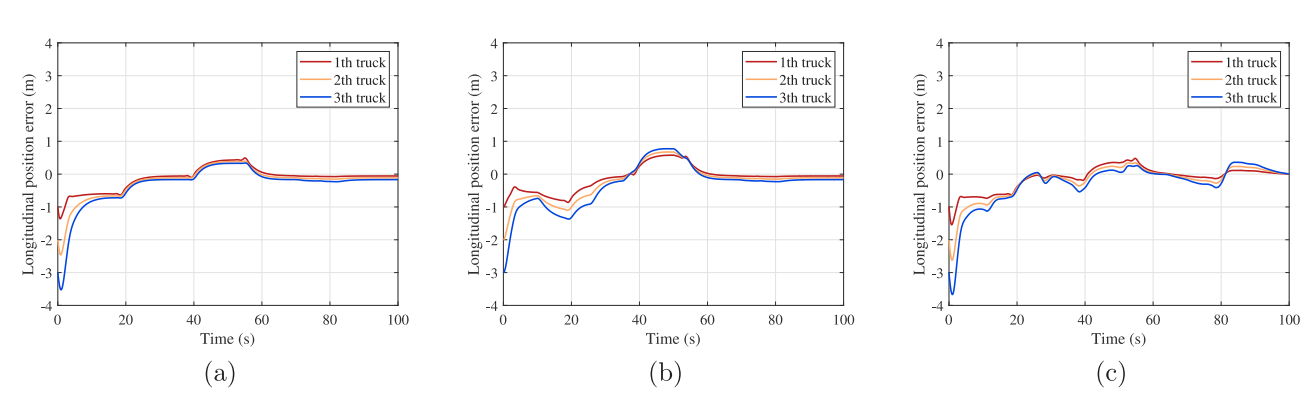


Fig. 21. Longitudinal spacing errors of following trucks: (a) constant speed, (b) speed setting, (c) RL-speed planning.

leading truck's velocity changes, the following trucks effectively track the curve. Fig. 21 presents the variation in the longitudinal spacing errors between each following truck and the leading truck. The results

indicate that the longitudinal spacing errors of the following trucks converge quickly, demonstrating that the controller ensures each following truck maintains good longitudinal tracking performance. Figs. 22 and

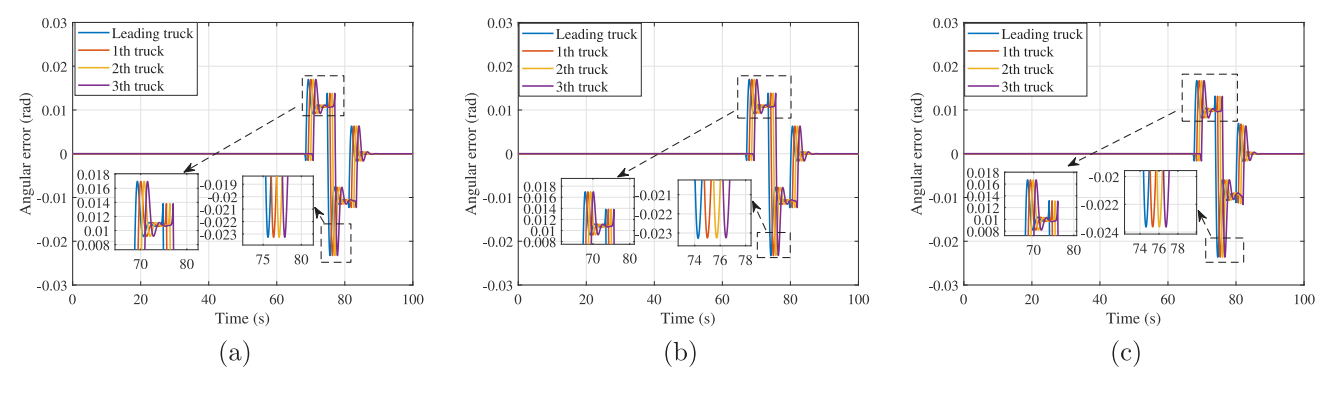


Fig. 22. Angular errors of trucks: (a) constant speed, (b) speed setting, (c) RL-speed planning.

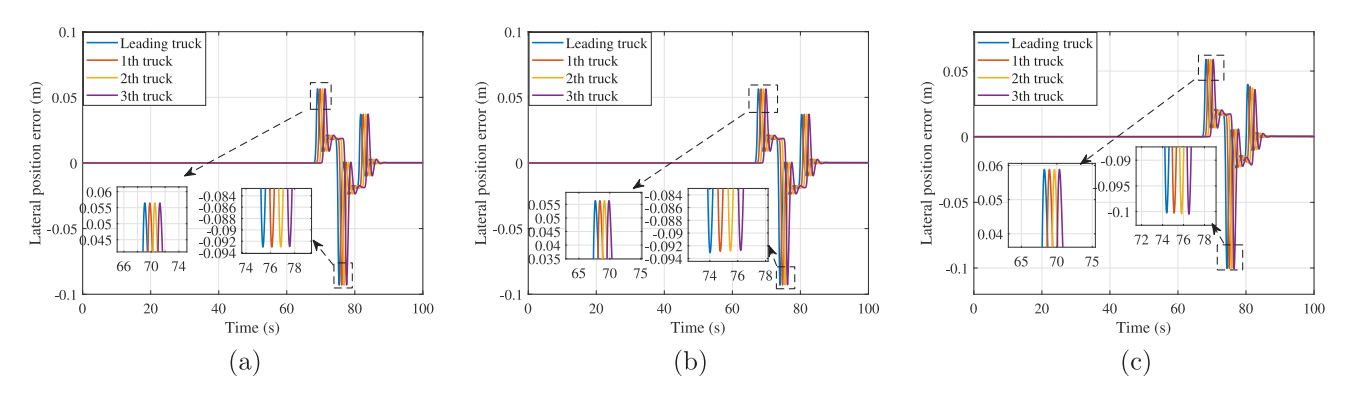


Fig. 23. Lateral position errors of trucks: (a) constant speed, (b) speed setting, (c) RL-speed planning.

23 display the angular errors and lateral position errors for each truck in the platoon under the three different scenarios. From these results, it is evident that the angular and lateral position errors of all trucks are small, thus meeting the control objectives.

Note that the superiority does not lie in the control performance. Instead, the real difference shows up in the fuel consumption, namely, the new method is more energy efficient.

Figs. 24 presents a comparative analysis of engine operating point distributions for the truck platoon under different strategies. As shown in Figs. 24(a), the proposed speed planning method results in most engine operating points concentrating within the region of minimum fuel consumption, demonstrating its effectiveness in optimizing power output and improving fuel economy.

In contrast, Fig. 24(b) illustrates the engine operating point distribution under a constant-speed driving strategy. Under this strategy, trucks require additional driving torque to maintain speed during uphill climbs due to gravitational resistance, while braking is needed downhill to prevent overspeeding. Consequently, the engine frequently operates outside the optimal efficiency zone.

Figs. 24(c) and 24(d) depict the engine operating point distributions for experience-based speed setting and RL-based speed planning methods, respectively. The experience-based method, relying on empirical formulations, lacks adaptive adjustment capabilities for real-world driving conditions, leading to a scattered distribution of engine operating points and suboptimal efficiency. Meanwhile, the RL approach, which can be viewed as an adaptive learning extension of the proposed speed planning method, autonomously adjusts speed strategies based on road conditions and powertrain demands, driving engine operation closer to the optimal fuel consumption region. A comparison of Figs. 24(a) to 24(d) confirms that the proposed speed planning method achieves superior energy-saving performance.

**Remark 8.** Note that the three trucks share identical physical parameters except for slight differences in mass, their operating points differ

marginally because the following trucks must compensate for spacing and tracking errors relative to the leading truck. This explains why their engine points cluster closely in the same high-efficiency region in Fig. 24.

Fig. 25 illustrates the fuel consumption histograms for the four methods. Based on speed planning fuel consumption data, it is clear that despite the greater mass of 1th following truck compared to the leading truck, there is still a fuel efficiency of about 5.1%, due to the significantly lower air resistance coefficient. 2th following truck can save about 7.14% on fuel compared to the first following truck, even with the same load. The air resistance coefficients of 2th following truck and 3th following truck are almost identical [71,72]. The fuel consumption slightly increases when the 3th following truck has a greater mass than 2th truck. Compared to total fuel consumption, speed planning can save 3.43%, 11% and 2.39% compared with constant speed, speed setting and RL-speed planning, respectively.

#### 6. Conclusion

In order to balance the fuel-saving and safety of truck platoons, this paper constructed a hierarchical strategy, including a speed planning layer and a platoon control layer. Firstly, the fuel-efficient velocity is determined based on the fuel consumption model, taking into account the tracking ability of the following trucks. Secondly, the DL-MPC was employed considering longitudinal and lateral coupling dynamics. Finally, co-simulation results revealed that the fuel consumption of the platoon based on speed planning was lower than that of constant speed, experience-based speed setting and RL-speed planning, where the energy-saving effect was illustrated by the fuel consumption characteristics of the engine. In addition, the performance of the iterative DL-MPC method was compared with the DMPC and TD3 methods in ensuring safety control of the platoon. It should be noted that the method proposed in this paper achieves a balance between the control performance and the computation time.

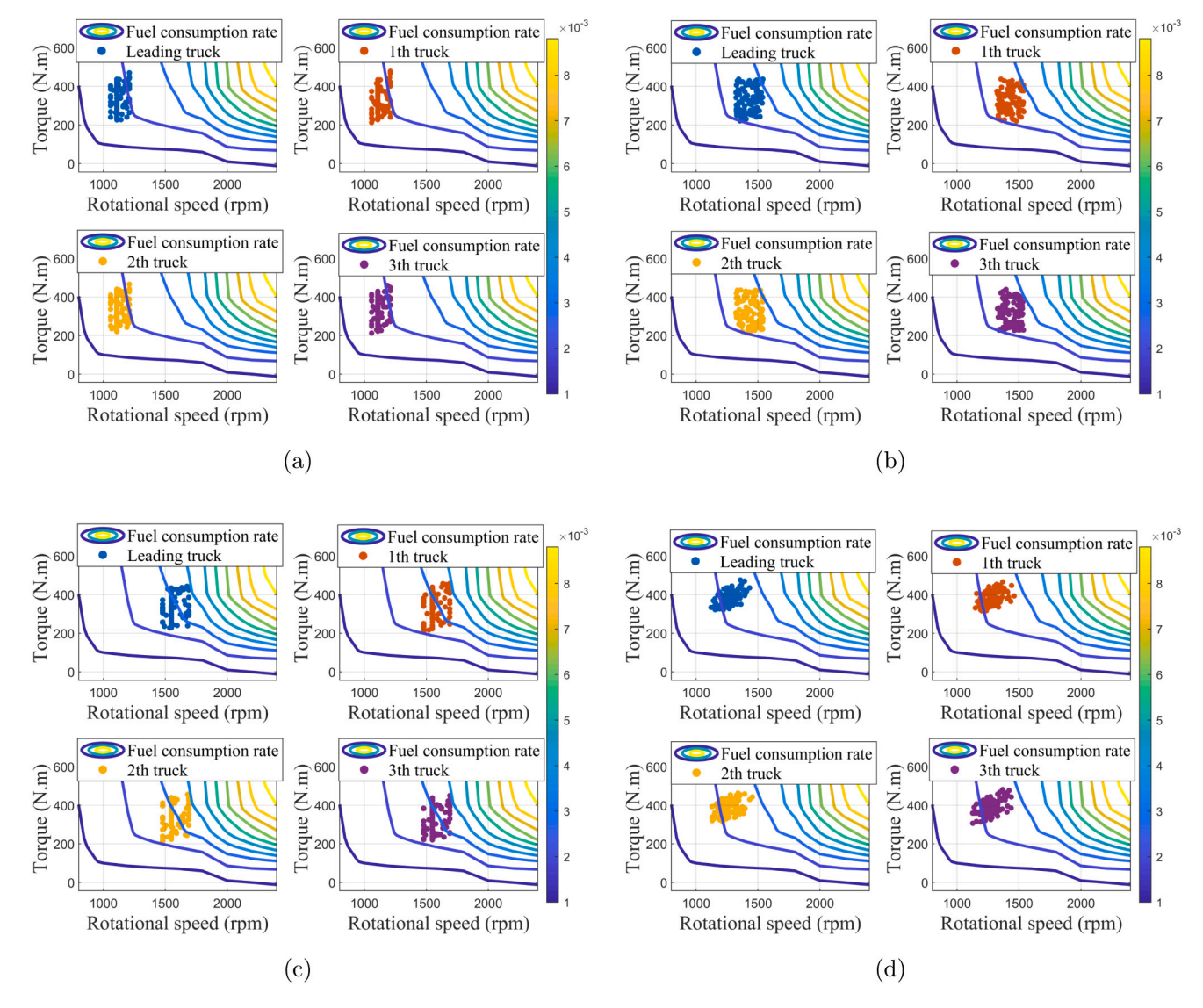


**Fig. 24.** Engine working point distribution map: (a) speed planning, (b) constant speed, (c) speed setting, (4) RL-speed planning. (The *y*-axis indeed represents the engine torque, the *x*-axis is the engine speed, and the background contour map indicates the fuel consumption rate.).

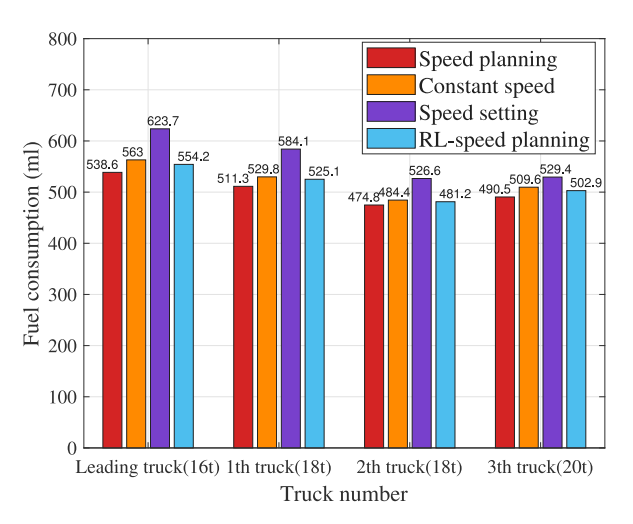


Fig. 25. Diagram of fuel consumption.

Beyond the specific application to truck platooning, the proposed DL-MPC framework has the potential to be extended to other cooperative control scenarios, such as automated transportation systems, smart grids, and unmanned aerial vehicle (UAV) platoons. In future work, platoon control will be investigated under more complex traffic environments, taking into account mixed traffic conditions, traffic signals, and uncertainties arising from vehicle dynamics. These studies aim to further enhance the robustness and practical applicability of the DL-MPC approach in real-world cooperative control systems.

## CRediT authorship contribution statement

**Shuyou Yu:** Writing – review & editing, Supervision, Project administration, Methodology, Investigation, Funding acquisition. **Shaoyu Sun:** Writing – original draft, Validation, Software, Investigation, Formal analysis. **Hong Chen:** Validation, Supervision. **Yangfan Liu:** Validation, Investigation. **Wenbo Li:** Supervision, Formal analysis, Conceptualization. **Jung-Su Kim:** Writing – review & editing, Data curation.

#### Declaration of competing interest

The authors declare that they have no known competing financial interests or personal relationships that could have appeared to influence the work reported in this paper.

#### Acknowledgments

This work is supported by the National Natural Science Foundation of China (No. 62473167) and the Natural Science Foundation of Jilin Province, China (No. 20240402079GH).

#### Data availability

Data will be made available on request.

#### References

- [1] Li Zihao, Zhou Yang, Zhang Yunlong, Li Xiaopeng. Enhancing vehicular platoon stability in the presence of communication cyberattacks: A reliable longitudinal cooperative control strategy. Transp Res Part C: Emerg Technol 2024;163:104660.
- [2] Lei Zhenzhen, Wan Wenjun, Xue Along, Zeng Chao, Zhang Yuanjian, Chen Zheng, Liu Yonggang. Energy efficiency optimization of passenger vehicles considering aerodynamic wake flow influence in car-following scenarios. Energy 2025:136501.
- [3] Ma Fangwu, Yang Yu, Wang Jiawei, Liu Zhenze, Li Jinhang, Nie Jiahong, Shen Yucheng, Wu Liang. Predictive energy-saving optimization based on nonlinear model predictive control for cooperative connected vehicles platoon with V2v communication. Energy 2019;189:116120.
- [4] Hu Jia, Wang Shuhan, Zhang Yiming, Wang Haoran, Liu Zhilong, Cao Guangzhi. Safety-aware human-lead vehicle platooning by proactively reacting to uncertain human behaving. Transp Res Part C: Emerg Technol 2025;170:104941.
- [5] Yao Zhihong, Wang Yi, Liu Bo, Zhao Bin, Jiang Yangsheng. Fuel consumption and transportation emissions evaluation of mixed traffic flow with connected automated vehicles and human-driven vehicles on expressway. Energy 2021;230:120766
- [6] Wang Zhong, Zhao Yahui, Zhang Yahui, Tian Yang, Jiao Xiaohong. Safe off-policy reinforcement learning on eco-driving for a P2-p3 hybrid electric truck. Energy 2024;313:133884.
- [7] Zhang Hailong, Peng Jiankun, Dong Hanxuan, Ding Fan, Tan Huachun. Integrated velocity optimization and energy management strategy for hybrid electric vehicle platoon: A multiagent reinforcement learning approach. IEEE Trans Transp Electrification 2023;10(2):2547–61.
- [8] Hu Manjiang, Li Chongkang, Bian Yougang, Zhang Hui, Qin Zhaobo, Xu Biao. Fuel economy-oriented vehicle platoon control using economic model predictive control. IEEE Trans Intell Transp Syst 2022;23(11):20836–49.
- [9] Liu Guanying, Guo Fengxiang, Liu Yonggang, Zhang Yuanjian, Liu Yu, Chen Zheng, Shen Shiquan. Weighted double Q-learning based eco-driving control for intelligent connected plug-in hybrid electric vehicle platoon with incorporation of driving style recognition. J Energy Storage 2024;86:111282.
- [10] Nie Zhigen, Zhu Lanxin, Jia Yuan, Lian Yufeng, Yang Wei. Hierarchical optimization control strategy for intelligent fuel cell hybrid electric vehicles platoon in complex operation conditions. Int J Hydrog Energy 2024;50:1056–68.
- [11] Li Wei, Song Ziyu, Ding Haitao, Xu Nan. Energy-efficient predictive and reactive control of connected electric vehicles platoon with string stability based on variable time headway. IEEE Trans Transp Electrification 2024;11(1):1970–83.
- [12] Zhang Qian, Guo Ge. Improved spacing policy-based predefined-time cooperative control of vehicles. IEEE Trans Veh Technol 2025;1–10.
- [13] Gao Yan, Li Dazhi, Sui Zhen, Tian Yantao. Trajectory planning and tracking control of autonomous vehicles based on improved artificial potential field. IEEE Trans Veh Technol 2024;73(9):12468–83.
- [14] Wang Shupei, Wang Ziyang, Jiang Rui, Zhu Feng, Yan Ruidong, Shang Ying. A multi-agent reinforcement learning-based longitudinal and lateral control of CAVs to improve traffic efficiency in a mandatory lane change scenario. Transp Res Part C: Emerg Technol 2024;158:104445.
- [15] Liu Jia, Cui Yunduan, Duan Jianghua, Jiang Zhengmin, Pan Zhongming, Xu Kun, Li Huiyun. Reinforcement learning-based high-speed path following control for autonomous vehicles. IEEE Trans Veh Technol 2024;73(6):7603–15.
- [16] Feng Yangyang, Yu Shuyou, Sheng Encong, Li Yongfu, Shi Shuming, Yu Jianhua, Chen Hong. Distributed MPC of vehicle platoons considering longitudinal and lateral coupling. IEEE Trans Intell Transp Syst 2023;25(3):2293–310.
- [17] Zhang Lin, Jiang Lianbo, Liu Hanghang, Hu Yunfeng, Wang Ping, Chen Hong. Coordinated longitudinal and lateral stability improvement for electric vehicles based on a real-time NMPC strategy. IEEE Trans Intell Transp Syst 2023;24(5):5337–50.

- [18] Liu Yalei, Ding Weiping, Yang Mingliang, Zhu Honglin, Liu Liyuan, Jin Tianshi. Distributed drive autonomous vehicle trajectory tracking control based on multi-agent deep reinforcement learning. Mathematics 2024;12(11):1614.
- [19] Gratzer Alexander L, Broger Maximilian M, Schirrer Alexander, Jakubek Stefan. Two-layer MPC architecture for efficient mixed-integer-informed obstacle avoidance in real-time. IEEE Trans Intell Transp Syst 2024;25(10):13767–84.
- [20] Zhou Quan, Du Changqing, Yan Yunbing, Chen Zhengfu. A tolerant sequential predictive energy management strategy for the platoon hybrid electric vehicle with the distributed driving optimization. Energy 2025;137921.
- [21] He Defeng, Luo Jie, Du Haiping. Dynamic negotiation-based distributed empc with varying consensus speeds of heterogeneous electric vehicle platoons. IEEE Trans Control Syst Technol 2024;32(4):1495–503.
- [22] Nie Zhigen, Jia Yuan, Wang Wanqiong, Chen Zheng, Outbib Rachid. Cooptimization of speed planning and energy management for intelligent fuel cell hybrid vehicle considering complex traffic conditions. Energy 2022;247:123476.
- [23] Tu Huizhao, Zhao Liying, Tu Ran, Li Hao. The energy-saving effect of early-stage autonomous vehicles: A case study and recommendations in a metropolitan area. Energy 2024;297:131274.
- [24] Tsugawa Sadayuki. Results and issues of an automated truck platoon within the energy its project. In: 2014 IEEE intelligent vehicles symposium proceedings. IEEE; 2014, p. 642–7.
- [25] Pan Chaofeng, Huang Aibao, Wang Jian, Chen Liao, Liang Jun, Zhou Weiqi, Wang Limei, Yang Jufeng. Energy-optimal adaptive cruise control strategy for electric vehicles based on model predictive control. Energy 2022;241:122793.
- [26] Li Meng, Cao Zehong, Li Zhibin. A reinforcement learning-based vehicle platoon control strategy for reducing energy consumption in traffic oscillations. IEEE Trans Neural Networks Learn Syst 2021;32(12):5309–22.
- [27] Kamal Md Abdus Samad, Mukai Masakazu, Murata Junichi, Kawabe Taketoshi. Ecological vehicle control on roads with up-down slopes. IEEE Trans Intell Transp Syst 2011;12(3):783–94.
- [28] Alam Assad, Mårtensson Jonas, Johansson Karl H. Look-ahead cruise control for heavy duty vehicle platooning. In: 16th international IEEE conference on intelligent transportation systems (ITSC 2013). IEEE; 2013, p. 928–35.
- [29] Kamal Md Abdus Samad, Mukai Masakazu, Murata Junichi, Kawabe Taketoshi. Model predictive control of vehicles on urban roads for improved fuel economy. IEEE Trans Control Syst Technol 2012;21(3):831–41.
- [30] Turri Valerio, Besselink Bart, Johansson Karl H. Cooperative look-ahead control for fuel-efficient and safe heavy-duty vehicle platooning. IEEE Trans Control Syst Technol 2016;25(1):12–28.
- [31] Guo Ge, Wang Qiong. Fuel-efficient en route speed planning and tracking control of truck platoons. IEEE Trans Intell Transp Syst 2018;20(8):3091–103.
- [32] Ozkan Mehmet Fatih, Ma Yao. Fuel-economical distributed model predictive control for heavy-duty truck platoon. In: 2021 IEEE international intelligent transportation systems conference. IEEE; 2021, p. 1919–26.
- [33] Dong Shiying, Chen Hong, Guo Lulu, Liu Qifang, Gao Bingzhao. Real-time energy-efficient anticipative driving control of connected and automated hybrid electric vehicles. Control Theory Technol 2022;20(2):210–20.
- [34] Lee Heeyun, Kim Kyunghyun, Kim Namwook, Cha Suk Won. Energy efficient speed planning of electric vehicles for car-following scenario using model-based reinforcement learning. Appl Energy 2022;313:118460.
- [35] Zhang Linlin, Chen Feng, Ma Xiaoxiang, Pan Xiaodong. Fuel economy in truck platooning: A literature overview and directions for future research. J Adv Transp 2020;2020(1):2604012.
- [36] Guo Jinghua, Li Keqiang, Luo Yugong. Coordinated control of autonomous four wheel drive electric vehicles for platooning and trajectory tracking using a hierarchical architecture. J Dyn Syst Meas Control 2015;137(10):101001.
- [37] Attia Rachid, Orjuela Rodolfo, Basset Michel. Combined longitudinal and lateral control for automated vehicle guidance. Veh Syst Dyn 2014;52(2):261–79.
- [38] Zhao Haiyan, Lu Xinghao, Chen Hong, Liu Qifang, Gao Bingzhao. Coordinated attitude control of longitudinal, lateral and vertical tyre forces for electric vehicles based on model predictive control. IEEE Trans Veh Technol 2021;71(3):2550-9.
- [39] Hu Jia, Wang Haoran, Li Xin, Li Xinghua. Modelling merging behaviour joining a cooperative adaptive cruise control platoon. IET Intell Transp Syst 2020;14(7):693-701.
- [40] Liu Peng, Kurt Arda, Ozguner Umit. Distributed model predictive control for cooperative and flexible vehicle platooning. IEEE Trans Control Syst Technol 2018;27(3):1115–28.
- [41] Huang Zichao, Chu Duanfeng, Wu Chaozhong, He Yi. Path planning and cooperative control for automated vehicle platoon using hybrid automata. IEEE Trans Intell Transp Syst 2018;20(3):959–74.
- [42] Jia Dongyao, Ngoduy Dong. Enhanced cooperative car-following traffic model with the combination of V2V and V2I communication. Transp Res Part B: Methodol 2016;90:172–91.
- [43] Park Hyungjun, Bhamidipati Chiranjivi Sarma, Smith Brian Lee. Development and evaluation of enhanced intellidrive-enabled lane changing advisory algorithm to address freeway merge conflict. Transp Res Rec 2011;2243(1):146–57.
- [44] Guan Hsin, Wang Bo, Lu Pingping, Xu Liang. Identification of maximum road friction coefficient and optimal slip ratio based on road type recognition. Chin J Mech Eng 2014;27(5):1018–26.

- [45] Aki Masahiko, Rojanaarpa Teerapat, Nakano Kimihiko, Suda Yoshihiro, Takasuka Naohito, Isogai Toshiki, Kawai Takeo. Road surface recognition using laser radar for automatic platooning. IEEE Trans Intell Transp Syst 2016;17(10):2800-10.
- [46] Liu Yonggui, Gao Huanli, Zhai Chunjie, Xie Wei. Internal stability and string stability of connected vehicle systems with time delays. IEEE Trans Intell Transp Syst 2020;22(10):6162–74.
- [47] Zhang Yuqin, Xu Zhihang, Wang Zijian, Yao Xinpeng, Xu Zhigang. Impacts of communication delay on vehicle platoon string stability and its compensation strategy: A review. J Traffic Transp Eng (English Edition) 2023;10(4):508–29.
- [48] Wang Pangwei, Deng Hui, Zhang Juan, Wang Li, Zhang Mingfang, Li Yongfu. Model predictive control for connected vehicle platoon under switching communication topology. IEEE Trans Intell Transp Syst 2021;23(7):7817–30.
- [49] Zhao Chengcheng, Cai Lin, Cheng Peng. Stability analysis of vehicle platooning with limited communication range and random packet losses. IEEE Internet Things J 2020:8(1):262–77.
- [50] Zhang Dan, Shen Ye-Ping, Zhou Si-Quan, Dong Xi-Wang, Yu Li. Distributed secure platoon control of connected vehicles subject to DoS attack: Theory and application. IEEE Trans Syst Man Cybern: Syst 2020;51(11):7269–78.
- [51] Mousavinejad Eman, Yang Fuwen, Han Qing-Long, Ge Xiaohua, Vlacic Ljubo. Distributed cyber attacks detection and recovery mechanism for vehicle platooning. IEEE Trans Intell Transp. Syst. 2019;21(9):3821–34.
- [52] Lyu Hao, Wang Ting, Cheng Rongjun, Ge Hongxia. Improved longitudinal control strategy for connected and automated truck platoon against cyberattacks. IET Intell Transp Syst 2022;16(12):1710–25.
- [53] Dang Dongfang, Gao Feng, Hu Qiuxia. Motion planning for autonomous vehicles considering longitudinal and lateral dynamics coupling. Appl Sci 2020;10(9):3180
- [54] Yan Maode, Ma Wenrui, Zuo Lei, Yang Panpan. Dual-mode distributed model predictive control for platooning of connected vehicles with nonlinear dynamics. Int J Control Autom Syst 2019;17(12):3091–101.
- [55] Chen Xiaolong, Zhou Bing, Wu Xiaojian. Autonomous vehicle path tracking control considering the stability under lane change. Proc Inst Mech Eng Part I: J Syst Control Eng 2021;235(8):1388–402.
- [56] Wang Xianbin, Shi Shuming, et al. Analysis of vehicle steering and driving bifurcation characteristics. Math Probl Eng 2015;2015.
- [57] Shi Shuming, Li Ling, Mu Yu, Chen Guanghui. Stable headway prediction of vehicle platoon based on the 5-degree-of-freedom vehicle model. Proc Inst Mech Eng Part D: J Automob Eng 2019;233(6):1570–85.
- [58] Wang Xianbin, Li Weifeng, Li Zhipeng, Li Zexuan, Zhang Fugang. Effect of braking torque on vehicle nonlinear dynamics. Meccanica 2023;58(7):1267–89.
- [59] Goeke Dominik, Schneider Michael. Routing a mixed fleet of electric and conventional vehicles. European J Oper Res 2015;245(1):81–99.

- [60] Yu Hwapyeong, Yeo Hwasoo. Traffic control policies for minimizing the negative effect of adaptive cruise control on highway. Transp Res Part C: Emerg Technol 2025:173:105063.
- [61] Li Shuai, Zheng Haotian, Wang Jiawei, Chen Chaoyi, Xu Qing, Wang Jianqiang, Li Keqiang. Influence of information flow topology and maximum platoon size on mixed traffic stability. Transp Res Part C: Emerg Technol 2025;171:104950.
- [62] Dunbar William B, Caveney Derek S. Distributed receding horizon control of vehicle platoons: Stability and string stability. IEEE Trans Autom Control 2011;57(3):620–33.
- [63] Zheng Yang, Li Shengbo Eben, Li Keqiang, Borrelli Francesco, Hedrick J Karl. Distributed model predictive control for heterogeneous vehicle platoons under unidirectional topologies. IEEE Trans Control Syst Technol 2016;25(3):899–910.
- [64] Haouari Bakhta, Mzid Rania, Mosbahi Olfa. A reinforcement learning-based approach for online optimal control of self-adaptive real-time systems. Neural Comput Appl 2023;1–27.
- [65] Duan Jingliang, Li Shengbo Eben, Liu Zhengyu, Bujarbaruah Monimoy, Cheng Bo. Generalized policy iteration for optimal control in continuous time. 2019, arXiv preprint arXiv:1909.05402.
- [66] Lian Chuanqiang, Xu Xin, Chen Hong, He Haibo. Near-optimal tracking control of mobile robots via receding-horizon dual heuristic programming. IEEE Trans Cybern 2015;46(11):2484–96.
- [67] Xu Xin, Chen Hong, Lian Chuanqiang, Li Dazi. Learning-based predictive control for discrete-time nonlinear systems with stochastic disturbances. IEEE Trans Neural Netw Learn Syst 2018;29(12):6202–13.
- [68] Mongillo Michael, et al. Choosing basis functions and shape parameters for radial basis function methods. SIAM Undergrad Res Online 2011;4(190–209):2–6.
- [69] Zhang Huaguang, Luo Yanhong, Liu Derong. Neural-network-based near-optimal control for a class of discrete-time affine nonlinear systems with control constraints. IEEE Trans Neural Netw 2009;20(9):1490–503.
- [70] Bai Linhan, Zheng Fangfang, Hou Kangning, Liu Xiaobo, Lu Liang, Liu Can. Longitudinal control of automated vehicles: A novel approach by integrating deep reinforcement learning with intelligent driver model. IEEE Trans Veh Technol 2024;73(8):11014–28.
- [71] Zhang Hanwen, Chen Jicheng, Zhu Chaojie, Zhang Hui. Deep learning-based energy-efficient spacing policy and platooning control co-design for connected and automated vehicles on inclined roads. IEEE Trans Veh Technol 2024;73(10):14486–98.
- [72] Hu Wenyu, Jiaqiang E, Han Dandan, Feng Changling, Luo Xiaoyu. Investigation on distribution characteristics of convective wind energy from vehicle driving on multi-lane highway. Energy 2023;271:127024.